Nontraumatic Intracranial Hemorrhage

Nancy J. Fischbein[a,*] and Christine A.C. Wijman[b]

KEYWORDS

• Intracranial hemorrhage • Cerebral amyloid angiopathy
• Vascular malformation • Venous infarction

Spontaneous or nontraumatic intracranial hemorrhage (ICH) accounts for approximately 10% to 15% of strokes in the United States. The hemorrhages are typically parenchymal, but may also primarily involve the subarachnoid space, subdural space, intraventricular space, or, rarely, epidural space. The clinical presentation of a parenchymal hemorrhage is usually with the sudden onset of a focal neurologic deficit, often accompanied by headache, alteration in the level of consciousness, seizure, and/or nausea and vomiting; intracranial extracerebral hemorrhage more typically presents with headache and alteration in the level of consciousness, although focal neurologic deficits may also be present, notably as a consequence of tissue shift and brain herniation.

The clinical presentations of ischemic stroke and ICH may be similar, and neuroimaging is indicated for further evaluation of the type of stroke and likely cause. Noncontrast computed tomography (CT) of the head is generally the first study performed on presentation to medical attention, because CT is rapid, widely available, and safe. CT is also highly sensitive to acute ICH, which appears dense compared with normal brain tissue and cerebrospinal fluid (CSF) (**Fig. 1**). Many institutions also perform CT angiography (CTA) and, less commonly, CT perfusion (CTP) as part of the assessment of acute ICH. MR with gradient-recalled echo (GRE) imaging is sensitive to acute hemorrhage, but MR (often with MR angiography [MRA], MR venography [MRV], and/or MR perfusion) is usually performed following CT to assess the cause of a known hemorrhage and to evaluate its effect on the rest of the brain parenchyma. In the setting of acute ischemic stroke with hemorrhagic transformation, MR with diffusion-weighted (DW) imaging is often key to making a diagnosis that could be missed on a noncontrast CT alone, and even on a CT that includes CTA and CTP, depending on the site and size of the infarct that underlies the hemorrhage. In the setting of spontaneous ICH, MR is generally most useful in assessing the cause of hemorrhage rather than the presence of hemorrhage itself; in addition, MR is sensitive to both acute and chronic hemorrhage, whereas CT is most sensitive to acute blood products.

The appearance of blood products is more complex on MR than on CT. On CT, acute blood is dense compared with brain tissue and CSF, and gradually decreases in density over days to weeks depending on the size of the hematoma. On MR, the appearance of the hematoma changes on T1- and T2-weighted images as the blood products evolve from oxyhemoglobin to eventually ferritin and hemosiderin.[1] The evolution of blood products on MR sequences is shown in **Fig. 2** and summarized in **Table 1**.[2,3]

The causes of nontraumatic ICH are numerous. This review focuses on the entities most commonly associated with nontraumatic ICH, such as hypertension and cerebral amyloid angiopathy (CAA),

[a] Department of Radiology (NF), Stanford University School of Medicine, Room S-047, 300 Pasteur Drive, Stanford, CA 94305-5105, USA
[b] Department of Neurology (CW), Stanford University School of Medicine, Stanford Stroke Center, 780 Welch Road, Suite 205, Stanford, CA 94305, USA
* Corresponding author.
E-mail address: fischbein@stanford.edu

Neuroimag Clin N Am 20 (2010) 469–492
doi:10.1016/j.nic.2010.07.003
1052-5149/10/$ – see front matter

Fig. 1. Axial nonenhanced CT scan shows a large dense hematoma (H) in the right frontal lobe. Only a small amount of vasogenic edema (*arrows*) is seen around this acute intraparenchymal hemorrhage.

but some increasingly recognized less common entities such as isolated cortical vein thrombosis, moyamoya disease, and the reversible cerebral vasoconstrictive syndrome are also discussed.

HYPERTENSIVE HEMORRHAGE

Long-standing hypertension is the leading cause of spontaneous intraparenchymal hemorrhage in adults. Pathophysiologically, long-standing hypertension leads to reactive hyperplasia of smooth muscle cells in cerebral arterioles. Eventually, smooth muscle death occurs, and vascular walls are replaced by collagen. Vascular occlusion or ectasia may then result, with either ischemic or hemorrhagic consequences. Hypertensive hemorrhages may also arise at sites of previous ischemic damage to the walls of small arteries and arterioles.[4]

Hypertensive hemorrhages tend to occur in the basal ganglia, thalami, cerebellum, and pons; the lobar white matter may also be affected (**Fig. 3**). A homogeneous, round or ovoid hematoma in one of these locations in an older adult patient has a high likelihood of being a result of the microangiopathy associated with long-standing uncontrolled hypertension. The age of the patient (whether older than 45 years or not), the presence of a history of hypertension, and the presence of certain associated imaging findings may help determine the yield of further imaging to assess for causes other than hypertension. On a CT scan, one may see evidence of microvascular ischemic change in the white matter as well as evidence of lacunar infarcts; these changes are common in the setting of chronic hypertension and increase the likelihood that hypertension is the underlying cause of the acute hemorrhage. On MR, one may also see evidence of white matter microvascular changes on fluid attenuated inversion recovery (FLAIR) and T2-weighted images, as well as evidence of prior lacunar infarcts or remote parenchymal hemorrhages. It is important to include a T2*-weighted sequence in the MR imaging protocol, because the presence of microbleeds in the brainstem and deep gray nuclei supports the likelihood of chronic hypertension and a hypertension-related hemorrhage (**Fig. 4**).[5] Brain hemorrhages related to drug abuse (typically cocaine and methamphetamine) may mimic the appearance of brain hemorrhages associated with long-standing hypertension on imaging studies, and likely share a common pathophysiology, but they tend to occur in a younger age group.

Intraparenchymal hematomas may expand by more than one-third of their original volume in up to 38% of patients who are imaged early.[6] Hematoma expansion most commonly occurs in the first few hours after symptom onset and has been associated with poor outcome. Risk factors for hematoma growth include time to initial CT scan (in that the earlier a patient is scanned after ICH onset, the more likely it is that the next CT will show ICH expansion), larger ICH volume on the initial CT, and oral anticoagulant use.[7] Other potentially important factors include hyperglycemia, renal failure, low serum cholesterol, platelet dysfunction, and persistently increased blood pressure.[8] On CTA and on the contrast-enhanced CT obtained after the CTA, the presence of focal contrast extravasation is associated with hematoma expansion,[9–11] providing potential justification for consideration of performing these studies on presentation to the hospital. Performing CTA can also help avoid the pitfall of misinterpreting hemorrhages caused by underlying pathologic conditions such as aneurysms or vascular malformations as hypertensive in patients who are older and who do have a diagnosis of hypertension (**Fig. 5**).

Supportive care (including blood pressure control and correction of coagulopathy) is the mainstay of management of acute intraparenchymal hemorrhage, with surgical evacuation having a more limited role in its management.[12] Most experts agree that cerebellar hematomas that are greater than 3 cm in diameter should be emergently evacuated if the patient is deteriorating neurologically or if the hematoma exerts mass effect on the brainstem or causes hydrocephalus. Furthermore,

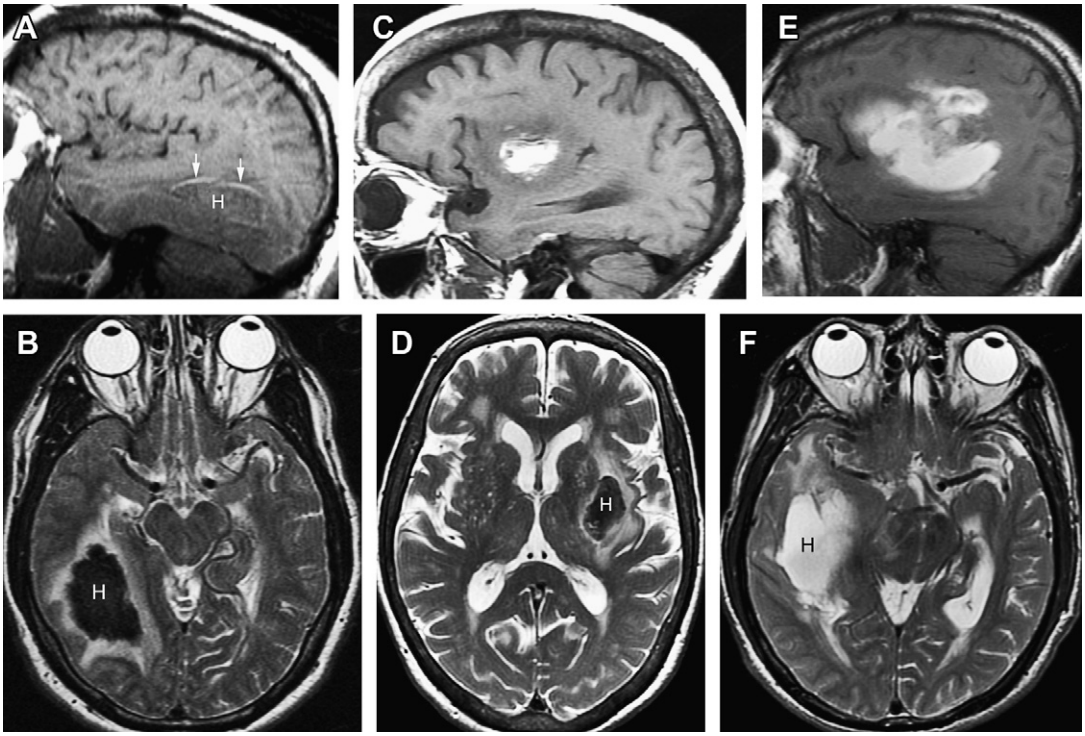

Fig. 2. Vertically paired images of acute, early subacute, and late subacute hematomas. (*A*) Sagittal T1-weighted (T1W) image shows an acute right temporal lobe hematoma (H) consisting largely of isointense deoxyhemoglobin. The beginning of transformation to methemoglobin along the periphery is seen as a thin bright line (*white arrows*). (*B*) Axial T2-weighted (T2W) image in the same patient shows low signal intensity because of deoxyhemoglobin in the hematoma (H). A surrounding rim of bright signal represents vasogenic edema. (*C*) Sagittal T1W image in a patient with an early subacute left subinsular/lateral putaminal hematoma shows high signal. (*D*) Corresponding T2W image shows central low signal intensity. This finding is consistent with intracellular methemoglobin in the hematoma (H). (*E*) Sagittal T1W image in a patient with a large right frontotemporal late subacute hematoma shows bright signal in the lesion. (*F*) Axial T2W image in the same patient also shows high signal in the hematoma (H), consistent with extracellular methemoglobin. There is surrounding vasogenic edema, as well as mass effect with uncal herniation and midbrain compression.

Table 1
MR imaging appearance of intraparenchymal hemorrhage

Timing	Blood Product	T1W Image	T2W Image
Hyperacute (<12 h)	Intracellular oxyhemoglobin	Isointense to hypointense	Hyperintense (variable hypointense rim)
Acute (hours to days)	Intracellular deoxyhemoglobin	Isointense	Hypointense
Subacute-early (few days)	Intracellular methemoglobin	Hyperintense	Hypointense
Subacute-late (week to months)	Extracellular methemoglobin	Hyperintense	Hyperintense
Chronic-early	Extracellular methemoglobin; ferritin/hemosiderin wall	Hyperintense	Hyperintense with low signal rim
Chronic-late	Hemosiderin	Isointense	Hypointense

Data from Refs.[1–3]

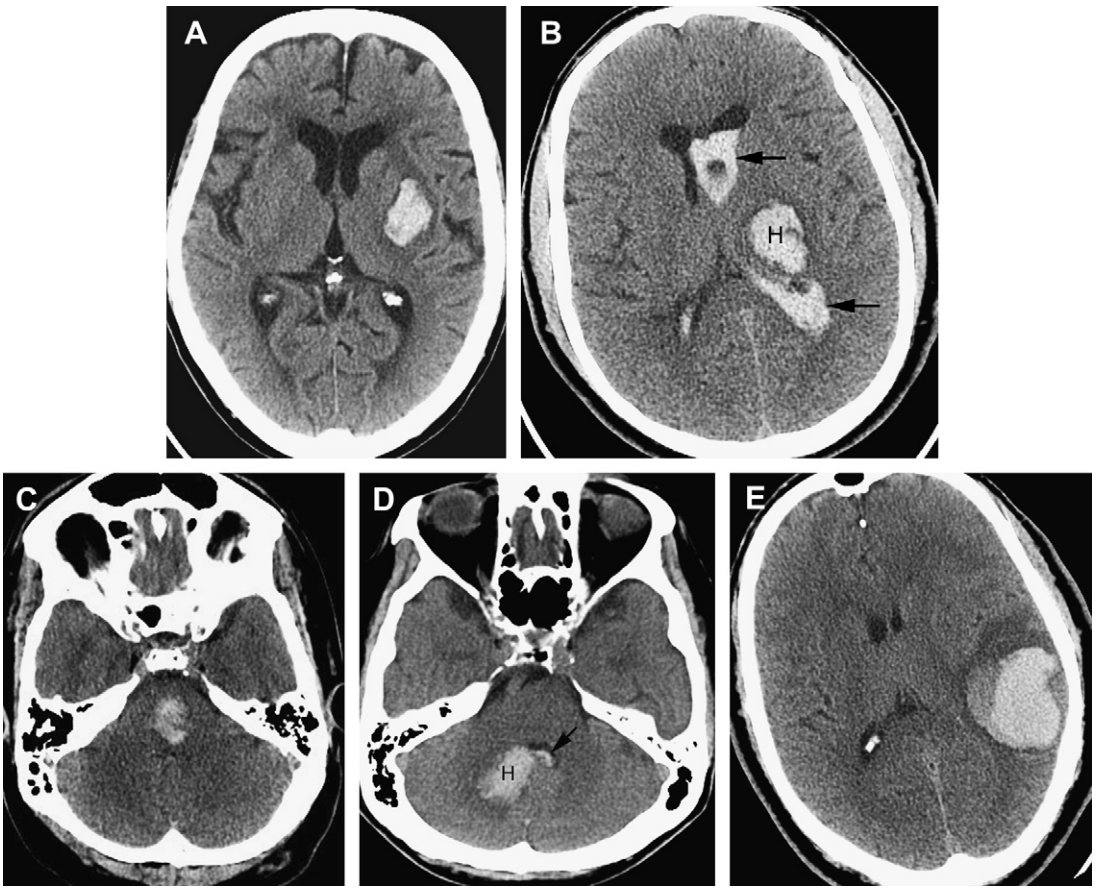

Fig. 3. Five different patients show the CT appearance of intraparenchymal hemorrhage associated with long-standing hypertension in the locations typically associated with hypertensive hemorrhage. (*A*) Acute hematoma in the left lateral putamen/external capsule. (*B*) Acute hematoma (H) in the left thalamus, complicated by intraventricular extension (*arrows*). (*C*) Acute hematoma in the central pons. (*D*) Acute hematoma (H) involving the deep white matter of the right cerebellum with extension into the fourth ventricle (*arrow*). (*E*) A large lobar hematoma with associated vasogenic edema. This location is less specific for ICH associated with long-standing hypertension and should raise concern for other potential causes, notably amyloid angiopathy in an elderly patient or tumor or vascular malformation in a younger patient.

based on the results of the International Surgical Trial in Intracerebral Hemorrhage (STICH), surgical evacuation may be considered for patients with superficial (<1 cm from the cortical surface) lobar hematomas.[13] Whether minimally invasive surgical techniques (using mechanical devices and/or endoscopy) to remove the hematoma offer benefit over conventional craniotomy/craniectomy is unknown and currently under investigation.

CEREBRAL AMYLOID ANGIOPATHY

CAA, a disorder that primarily affects individuals older than 60 years, is defined by the accumulation of amyloid in the walls of small and medium-sized cerebral arteries within the brain and leptomeninges. Both inherited and sporadic forms of CAA exist; the inherited form is less common, has an earlier onset of symptoms, and is more strongly associated with dementia.[14] Amyloid deposition in cerebral blood vessels can have several clinical consequences. First, it may be asymptomatic, as it is known that more than 50% of individuals older than 80 years have pathologic evidence of CAA. Second, it may weaken the vessel wall, leading to a rupture and ICH. Third, it can obliterate the vascular lumen, leading to ischemia and contributing to leukoencephalopathy.[15]

CAA-related hemorrhages are said to account for 5% to 20% of nontraumatic cerebral hemorrhages in elderly patients, so it is second only to hypertension as a cause of spontaneous ICH. The hallmark of the CAA-related hemorrhage is a lobar, cortical,

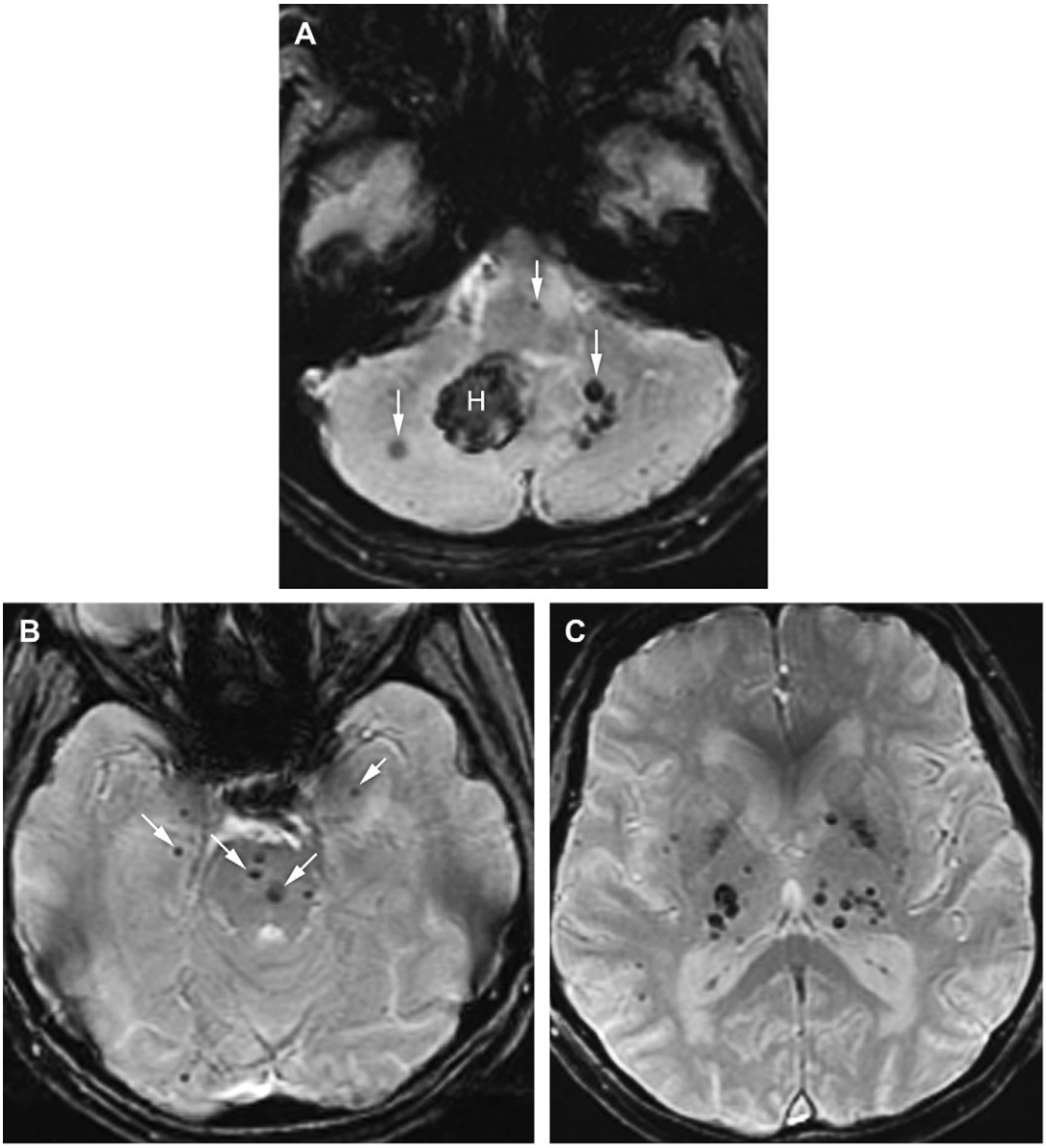

Fig. 4. (*A*) Axial GRE image through the posterior fossa in a patient with a cerebellar hemorrhage (H) shows multifocal microhemorrhages (*arrows*) related to chronic hypertension. (*B*) A more superior GRE image in the same patient shows microhemorrhages in the pons as well as a few scattered microhemorrhages in the temporal lobes. (*C*) An axial GRE image at the level of the deep gray nuclei shows numerous microhemorrhages with a thalamic predilection. This deep and central distribution of microhemorrhages is typical of chronic severe and uncontrolled hypertension.

or cortical-subcortical hemorrhage affecting normotensive individuals older than 55 years; the hemorrhages are frequently multiple and recurrent, and often extend to the subarachnoid space.[16] An important clue to the diagnosis of CAA is the presence of multiple petechial hemorrhages (microbleeds) in characteristic locations identified on T2*-weighted MR images (Fig. 6). Unlike the microbleeds associated with chronic hypertension, which are typically located in the brainstem and deep gray nuclei, the microbleeds of CAA tend to be located peripherally in the cerebellum and in the cortical-subcortical region of the cerebral hemispheres. Newer MR imaging methods such as susceptibility-weighted imaging are exquisitely sensitive to chronic blood products and will likely increase the frequency of diagnosis of CAA and other hemorrhagic disorders in coming years, as will the

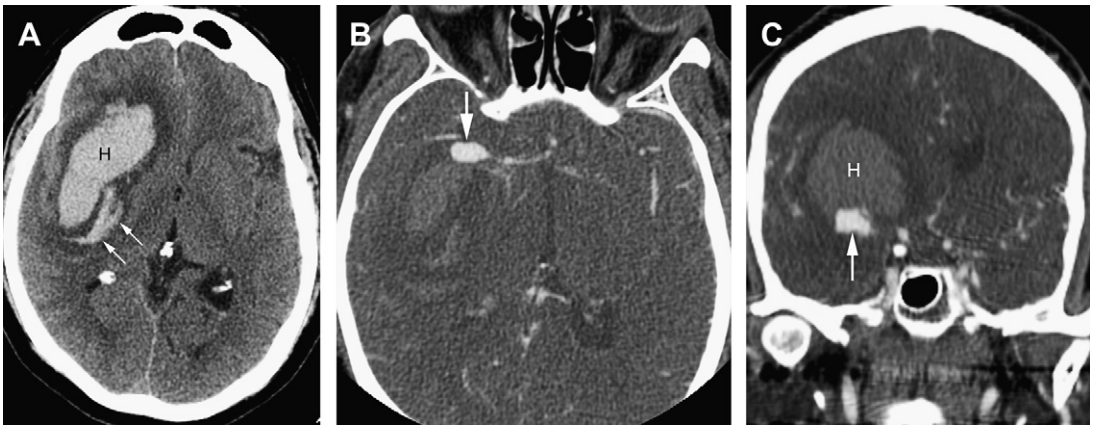

Fig. 5. (*A*) Axial NECT image shows a large lobar hematoma (H) with mild surrounding edema and associated mass effect in a 53-year-old man with a history of chronic hypertension. The hematoma is somewhat heterogeneous along its medial aspect (*arrows*), and it extends more anteriorly than a typical basal ganglia/external capsule hypertensive hemorrhage, but this lesion could potentially be diagnosed as a hemorrhage associated with long-standing hypertension. (*B*) An axial image from a CTA shows a lobulated, contrast-filled mass consistent with a saccular aneurysm arising from the right MCA. (*C*) A coronal maximum-intensity projection (MIP) image shows the relationship of the inferiorly located MCA aneurysm (*arrow*) to the more superior hematoma (H).

increasing prevalence of high-field (3 T and greater) imaging systems.[17]

The use of warfarin in patients with CAA is controversial. Warfarin use is associated with an annual ICH risk of 0.3% to 0.6%, and risk factors for warfarin-associated ICH include older age, leukoaraiosis, and CAA. Given the associated stroke risk of 5% to 12% per year with atrial fibrillation and 4% per year in patients with mechanical valves, most clinicians choose to place patients with atrial fibrillation or mechanical heart valves on chronic warfarin therapy despite imaging

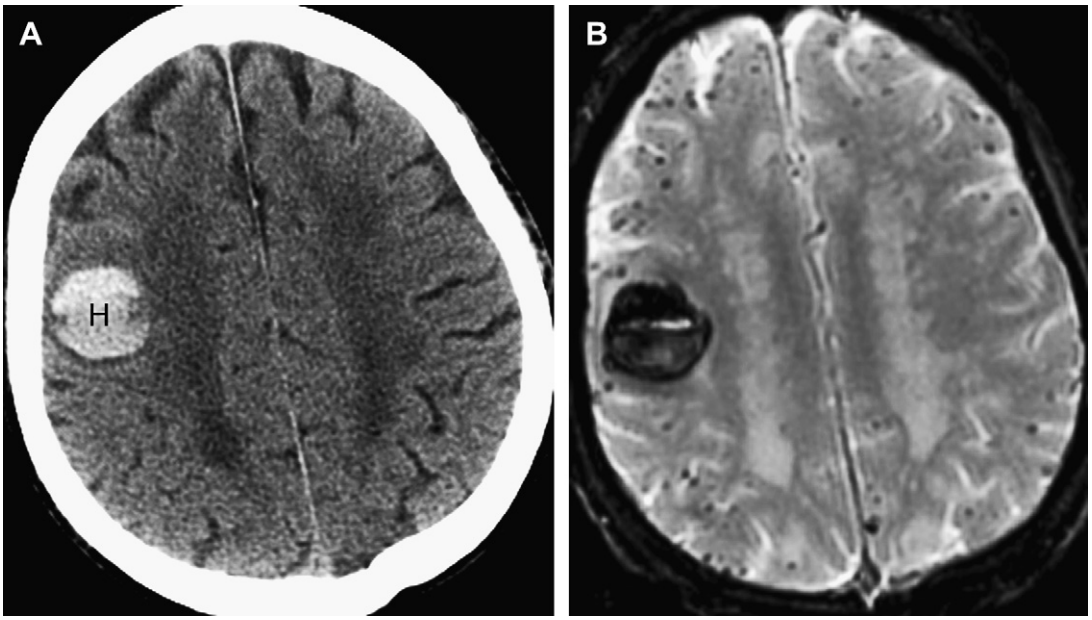

Fig. 6. (*A*) Axial NECT image in an elderly patient shows an acute right frontal lobar hematoma (H). The white matter shows diffuse hypodensity consistent with chronic microvascular ischemic change. (*B*) Axial GRE image shows the right frontal hematoma but also shows innumerable peripherally located microhemorrhages. This GRE appearance is classic for CAA.

evidence of an increased risk of warfarin-associated ICH in patients with CAA. In patients who have suffered a warfarin-associated ICH, the risk of subsequent cardioembolic complications needs to be weighed against the risk of ICH recurrence.[18]

HEMORRHAGIC TRANSFORMATION OF ISCHEMIC STROKE

Hemorrhagic transformation of an ischemic stroke (HTIS) can be misdiagnosed as a primary intraparenchymal hemorrhage if the underlying ischemic infarct is not appreciated from clinical or imaging evaluation, but in most cases it is readily recognized as a complication of prior arterial infarction (**Fig. 7**). HTIS has been associated with baseline stroke severity, hyperglycemia, uncontrolled hypertension,[19] advanced age, use of thrombolytics, nonrecanalization, and use of anticoagulants, among other risk factors.[20–22] HTIS may be evident on imaging studies alone (usually petechial hemorrhage), or may cause deterioration of a patient's clinical condition (parenchymal hematoma). HTIS is reported as complicating from 2% to 40% of ischemic strokes, depending how carefully one looks for it with various imaging modalities. Symptomatic intracerebral hemorrhage in the setting of ischemic infarction treated with intravenous or intraarterial thrombolytic therapy occurs in only approximately 6% to 12% of patients.

Predicting which ischemic strokes may undergo hemorrhagic transformation is of interest as use of thrombolytic agents becomes more widespread and as these agents are more frequently administered in later time windows (eg, more than 4.5 hours after symptom onset). Radiographic risk factors for hemorrhagic transformation after thrombolytic therapy include large areas of hypoattenuated brain parenchyma and a hyperdense middle cerebral artery (MCA) sign on the pretreatment head CT.[23,24] In addition, patients who do not recanalize are at higher risk for subsequent hemorrhage. On CTP, the permeability-surface area product has been suggested to be useful in identifying patients with acute ischemic stroke who are likely to develop hemorrhagic transformation.[20] On MR, a malignant pattern of large regions of DW and perfusion-weighted imaging abnormality combined with early reperfusion seemed to predict symptomatic hemorrhagic transformation and poor clinical outcome.[21,25] In addition, the cause of ischemic stroke influences whether hemorrhagic transformation occurs. Septic emboli, especially those of fungal cause, are often accompanied by parenchymal hemorrhage, and this diagnosis should be strongly considered in the appropriate clinical setting when a patient presents with multifocal ischemic infarcts associated with hemorrhage (**Fig. 8**).[26] Ischemic stroke is discussed in greater detail in the article Imaging of Ischemic Stroke by Leiva-Salinas and Wintermark elsewhere in this issue.

ANEURYSMAL SUBARACHNOID HEMORRHAGE

The most common cause of subarachnoid hemorrhage (SAH) is trauma, but aneurysmal SAH accounts for at least 85% of nontraumatic SAH

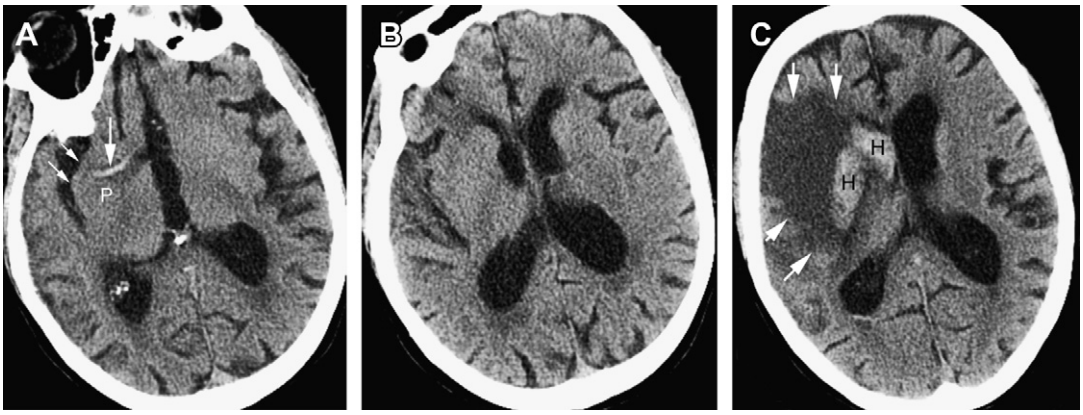

Fig. 7. (*A*) Axial NECT image from an elderly woman with acute onset of left hemiparesis shows a dense MCA (*large white arrow*), consistent with clot in the vessel. Signs of early arterial infarction are present, with subtle hypodensity in the right insular ribbon (*arrows*) and inferior putamen (P). (*B*) A more superior axial CT image from the same study shows subtle hypodensity in the right corpus striatum, as well as the insula and right frontal lobe; there is mass effect on the right lateral ventricle. (*C*) A follow-up NECT 3 days later shows hemorrhagic transformation (H) involving right caudate and putamen, as well as increasing hypodensity in the evolving right frontal infarct. There is increased mass effect on the right frontal horn, and a small amount of intraventricular hemorrhage.

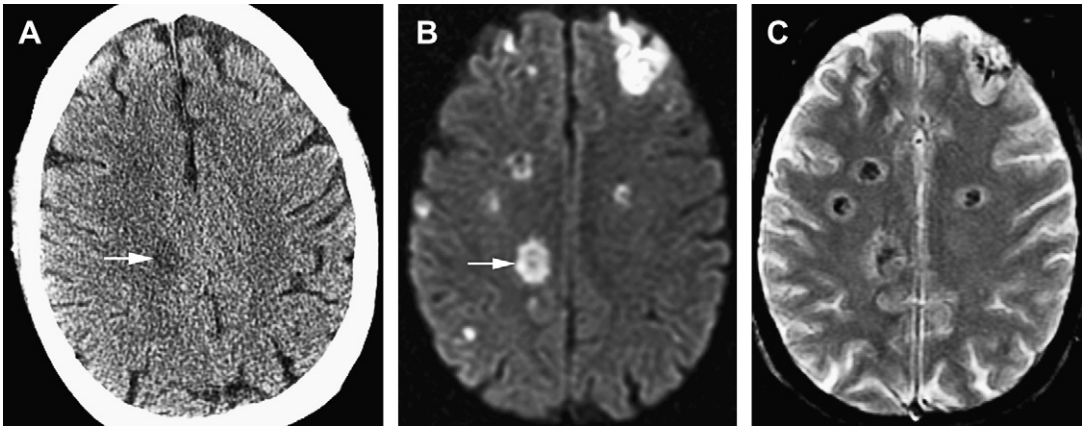

Fig. 8. (*A*) Axial NECT in a 56-year-old man after bone marrow transplant for leukemia and with new left-sided weakness shows a nonspecific hypodense lesion in the right centrum semiovale. (*B*) A brain MR image with DW imaging performed the following day shows multifocal rounded and also wedge-shaped areas of reduced diffusion, with a right posterior frontal lesion (*arrow*) corresponding to the lesion seen on the CT scan. (*C*) An axial GRE image at the same level shows that many of the lesions have central hypointensity consistent with hemorrhage. Biopsy confirmed hemorrhagic septic emboli caused by aspergillosis.

cases. Aneurysmal SAH accounts for only 5% of stroke cases, but with an associated mortality of 12% to 66% in various studies, this stroke subtype accounts for the most life-years lost to stroke.[27] Common risk factors for aneurysmal SAH are hypertension and smoking, and it affects women more frequently than men. Patients with aneurysmal SAH typically present with acute onset of severe headache, often described as the worst headache of the patient's life. Other symptoms and signs may include vomiting, seizures, nuchal rigidity, cranial nerve palsies, and alteration in the level of consciousness ranging from confusion and drowsiness to coma. The diagnosis of acute SAH is made on noncontrast CT, or by lumbar puncture when the CT scan is negative and clinical suspicion is high. The likelihood of missing acute SAH on the initial CT scan increases as the time interval between symptom onset and time of the CT scan increases. Once nontraumatic SAH has been diagnosed, the patient usually undergoes an urgent evaluation focused on identifying the cause of the SAH: saccular aneurysms are the most common cause, but dissecting intracranial aneurysms and vascular malformations (discussed in detail later) may also present with spontaneous SAH.

On nonenhanced CT (NECT) imaging, aneurysmal SAH typically presents as increased density in the basal cisterns and/or Sylvian fissures. The pattern of hemorrhage may provide insight into the likely location of the aneurysm (ie, blood in the anterior interhemispheric fissure is associated with rupture of an anterior communicating artery aneurysm). Some patients may have an intraparenchymal hematoma in addition to blood in the subarachnoid space, and the hematoma is typically adjacent to the dome of the aneurysm. In some cases the offending aneurysm may be large enough to be identified as a mass on an NECT, or it may be seen as a relative filling defect within the dense cisternal blood; calcified aneurysms can also be identified on NECT. The most common locations for saccular aneurysms include the anterior communicating artery, posterior communicating artery, and MCA trifurcation, but many other locations (basilar tip, posterior inferior cerebellar artery, anterior choroidal artery) may also be seen.

In the past, urgent catheter angiography was generally indicated for assessment of nontraumatic SAH. In the past decade, however, CTA has evolved as the initial study of choice in many centers (**Fig. 9**). On CTA, the typical saccular aneurysm is seen as a rounded contrast-filled outpouching of the vessel wall. It is important to scrutinize both the source images and the three-dimensional (3D) reformations of the CTA carefully, because in some cases one or the other of these image sets may show the aneurysm to better advantage.

CTA can be acquired quickly and easily even in acutely ill patients, and it has a high level of diagnostic accuracy: modern multislice CT scanners have been reported to provide a sensitivity, specificity, and accuracy as high as 100% even for small aneurysms (5 mm or less) in multiple series.[27–29] Contraindications to CTA include allergy to iodinated contrast material and renal insufficiency; in addition, CTA can be degraded by patient motion

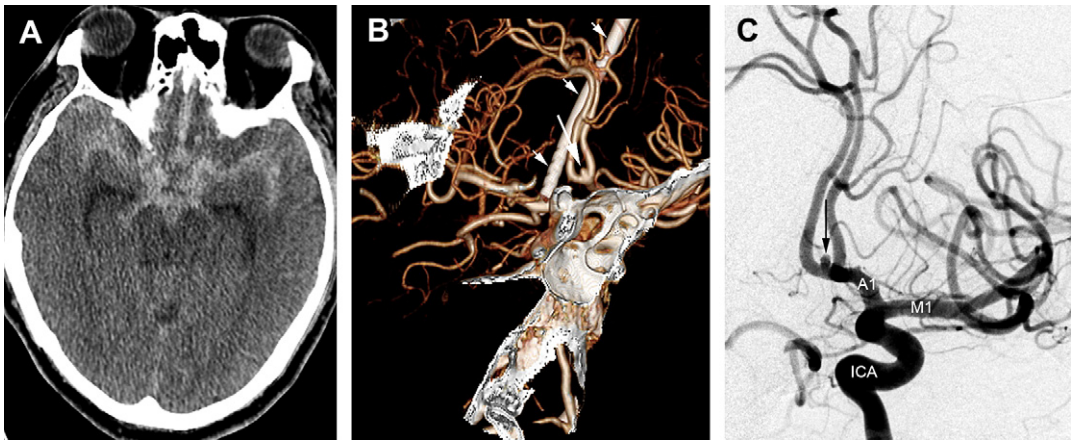

Fig. 9. (*A*) Axial NECT shows diffuse acute SAH in the suprasellar cistern, anterior interhemispheric fissure, and Sylvian fissures. Mild hydrocephalus is present, with dilatation of the temporal horns. (*B*) Oblique view of a 3D volume-rendered image from a CTA shows a saccular aneurysm of the anterior communicating artery (*large white arrow*). An intraventricular drain is also in place (*short white arrows*). (*C*) An anterioposterior view from a catheter angiogram with left ICA injection confirms the presence of the small saccular aneurysm arising from the anterior communicating artery. Also indicated are the A1 and M1 segments of the left anterior and middle cerebral arteries.

and a poor quality bolus (because of technical factors or patient factors such as poor cardiac output). CTA can also be a significant source of radiation exposure, especially if multiple studies are performed. If clinical suspicion of aneurysmal SAH is high and CTA is negative, then assessment with digital subtraction angiography (DSA), preferably accompanied by 3D rotational angiography, should be strongly considered.[30] Furthermore, although many surgeons proceed to the operating room from CTA alone, DSA may be indicated for preoperative assessment of complex aneurysms and for assessment of the presence of additional asymptomatic aneurysms. MRI/MRA may be used in selected situations for the assessment of aneurysmal SAH, but high signal intensity of the CSF on FLAIR is not specific for hemorrhage, and areas of poor CSF suppression limit overall sensitivity to hemorrhage in the subarachnoid space; MRI/MRA also takes longer than CTA, making the MR scanner a less optimal environment for a critically ill patient than the CT scanner.[31] Safety concerns regarding the MR environment also make it less appropriate for critically ill patients in whom appropriate MR safety screening cannot be performed.

Once an aneurysm has been identified, then the course of treatment is dictated to a large extent by the precise anatomy of the aneurysm, the clinical condition of the patient, the preferences of patient and family, and the availability of neurosurgical and neurointerventional services, as both surgical clipping and endovascular coiling of aneurysms are in routine clinical use. If a patient survives the initial aneurysm rupture, then he/she must be carefully watched for the development of vasospasm; angiographic vasospasm occurs in approximately 70% of patients who survive the initial rupture, and about half of these patients develop neurologic deficits. Clinical and transcranial Doppler monitoring for development of vasospasm can often be effectively supplemented with CTA,[32] thereby avoiding unnecessary DSA in many cases, although DSA is necessary for intraarterial therapy for vasospasm. The treatment of aneurysms and aneurysmal SAH is discussed in more detail in the article Acute Neuro-Interventional Therapies by Hetts and English elsewhere in this issue.

VASCULAR MALFORMATIONS

Vascular malformations account for approximately 20% of spontaneous ICHs and are the leading cause of spontaneous ICH in young adults.[33] Vascular malformations include arteriovenous malformations (AVMs), dural arteriovenous fistulas (dAVFs), cavernous malformations (CMs), developmental venous anomalies (DVAs), and capillary telangiectasias, with AVMs and CMs accounting for most of the clinically evident hemorrhages.

An AVM is a developmental lesion characterized by abnormal connections between pial arteries and veins with no intervening capillary

bed; the feeding arteries are usually branches of the internal carotid or vertebrobasilar system, and the AVM is typically located in the brain parenchyma. A central nidus that varies in size from microscopic to several centimeters represents the site of anomalous connection, and in larger lesions, enlarged feeding arteries and draining veins can be seen extending to and away from the central nidus. In the absence of hemorrhage most patients are asymptomatic, although some may have headaches or seizures that bring them to medical attention, and some AVMs are incidentally detected on imaging studies performed for other indications; however,

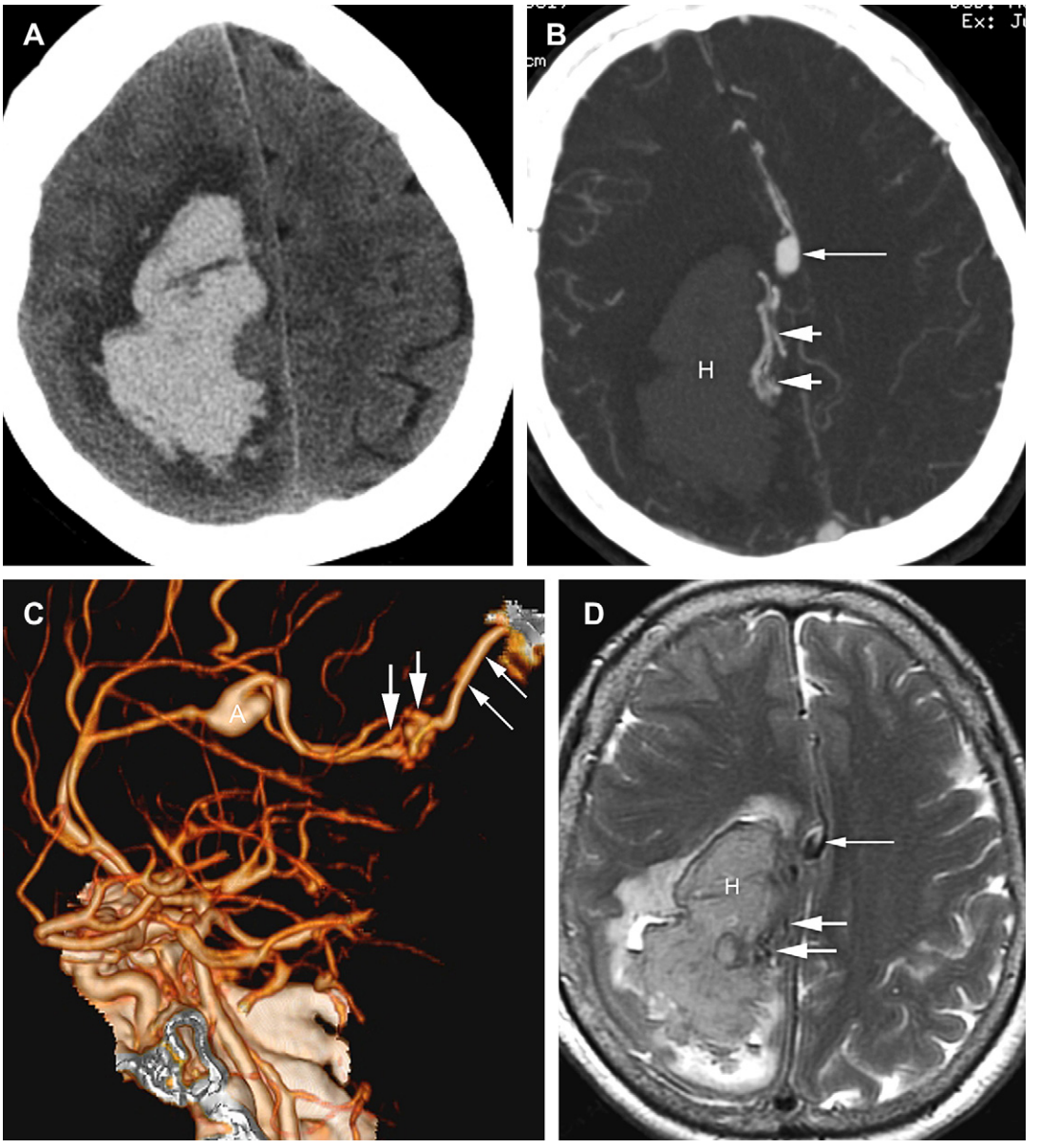

Fig. 10. (*A*) Axial NECT shows a large lobar hematoma with surrounding edema in a 69-year-old woman. (*B*) An axial MIP image from a CTA shows a nidus of abnormally enlarged vessels (*short white arrows*), consistent with an arteriovenous malformation located along the medial aspect of the hematoma (H). The thin long arrow indicates a feeding artery aneurysm arising from the right anterior cerebral artery. (*C*) A 3D volume-rendered image from the CTA in a roughly sagittal projection shows the feeding artery aneurysm (*A*), the nidus of the AVM (*thick white arrows*), and the dominant draining vein (*thin white arrows*). (*D*) An axial T2W image from an MR scan performed shortly after the CTA shows the large hematoma (H), as well as the anterior cerebral artery (ACA) aneurysm (*long arrow*) and the subtle flow voids associated with the nidus of the AVM (*thick white arrows*).

hemorrhage is often the initial clinical presentation of AVM.

On a noncontrast CT scan, an AVM associated with ICH may be recognized because of enlarged, serpiginous, dense feeding arteries and/or draining veins; there may also be encephalomalacia and/or mineralization of the adjacent brain parenchyma. On CTA, the abnormal vessels usually can be directly visualized (**Fig. 10**). Similarly, if MRI/MRA is performed, then abnormal vessels also may be directly visualized. Catheter angiography is used to diagnose small AVMs that may be occult on both CT and MR, to fully characterize an AVM, and often for therapeutic intervention. In rare instances, AVMs may be occult even on contrast angiography, generally because the abnormal vessels are compressed in the acute phase by hematoma. Repeat angiography in the chronic phase after resorption of the hematoma is appropriate in selected patients with a high index of suspicion and a negative initial cerebral angiogram. Once an AVM has been identified, treatment is often multimodality depending on the complexity of the lesion; transcatheter embolization, surgical resection, and stereotactic radiosurgery may all play a role in AVM management. The well-known Spetzler and Martin grading system for AVMs is summarized in **Table 2** and attempts to predict the risk of surgical morbidity and mortality by assigning points to an AVM from several lesion characteristics.[34]

Table 2
Spetzler-Martin grading system for arteriovenous malformation

Graded Feature[a]	Points Assigned
Size of AVM (cm)	
Small (<3)	1
Medium (3 to 6)	2
Large (>6)	3
Eloquence of adjacent brain	
Noneloquent	0
Eloquent	1
Pattern of venous drainage	
Superficial only	0
Deep	1

[a] Grade, sum of points assigned in each of the 3 categories, and so ranges from I to V.

Data from Spetzler RF, Martin NA. A proposed grading system for arteriovenous malformation. J Neurosurg 1986;65:476–83.

CMs affect 0.2% to 0.4% of the population, but the frequency of associated clinically evident ICH is far lower.[35] CMs are considered vascular hamartomas; these low-flow lesions consist of closely apposed endothelial-lined blood vessels without intervening brain tissue. CMs may be found in any region of the brain, and they may occur in isolation, in association with a DVA, or as part of a genetic syndrome in which numerous CMs are present. CMs may be associated with acute ICH, but many come to attention because of headache or seizure, or they are detected incidentally on imaging studies performed for unrelated indications.

On CT, CMs are often difficult to appreciate, although they may be seen as small (usually 1 cm or smaller, although some are as large as 5 cm or more), round or ovoid areas of subtle hyperdensity caused by mineralization and blood products. If a CM has recently bled, then the acute hemorrhage may be evident on the CT scan. On MR, CMs are characterized by a mixed signal intensity core with areas that are typically bright on both T1- and T2-weighted images, and a low signal intensity rim (**Fig. 11**). The hemosiderin rim is especially well appreciated on GRE sequences, and often a small CM is detectable only on this sequence. Gadolinium is usually given to look for an associated developmental venous anomaly (DVA). This is also very useful in the setting of acute hemorrhage: the underlying CM may be obliterated or compressed by an acute hematoma, but if a DVA can be identified in proximity to the hematoma, then CM is likely the underlying cause of the hemorrhage. CMs are typically angiographically occult, and catheter angiography does not play a role in their diagnostic evaluation or management.

dAVFs are a heterogeneous group of lesions that share the common feature of arteriovenous shunting within the dura: an abnormal direct connection (fistula) is present between a meningeal artery and a meningeal vein or dural venous sinus.[36] These lesions represent 6% of supratentorial and 35% of infratentorial vascular malformations. They are typically acquired and idiopathic, although some may be associated with antecedent events such as prior dural sinus thrombosis, craniotomy, or trauma[37]; rarely these lesions are congenital. They may occur at any level of the brain, skull base, and spine, but intracranially they are most common at the level of the cavernous sinus and in the posterior fossa. Several classification systems exist for dAVF, and the commonly used systems are summarized in **Table 3**.[38,39] These classification systems help to stratify patients according to their risk of hemorrhagic complications related to the underlying dAVF.

dAVFs may present with ICH or progressive neurologic deficits. Venous hypertension may lead to localized symptoms such as pulsatile tinnitus or cavernous-orbital syndrome depending on the precise location and drainage characteristics of the fistula, or may lead to more generalized and diffuse symptoms such as intracranial hypertension and dementia. Spontaneous ICH may also be a presenting symptom, usually in patients in whom antegrade drainage is obstructed and cortical venous drainage is present. NECT may be normal if the patient does not have ICH or hydrocephalus, but in some patients abnormal dural sinuses or transosseous vascular channels may be noted. Contrast-enhanced CT and CTA may show abnormally enlarged and tortuous feeding arteries, enlarged or occluded dural sinuses, and enlarged cortical draining veins depending on the precise angioarchitecture of the fistula (**Fig. 12**). MRI/MRA/MRV may show similar imaging features, and dynamic MRA may be particularly useful in fistula identification and characterization.[40] Catheter angiography plays several essential roles in the evaluation and management of dAVFs:

1. Diagnosis: the lesions may be subtle or occult on noninvasive imaging studies
2. Characterization: angiography allows complete assessment of arterial input and venous drainage
3. Treatment: many dAVFs can be treated partially or completely with endovascular methods.

DVAs and capillary telangiectasias do not typically present with ICH (except as discussed earlier, when CMs occur in association with DVAs) and are not further discussed in this article.

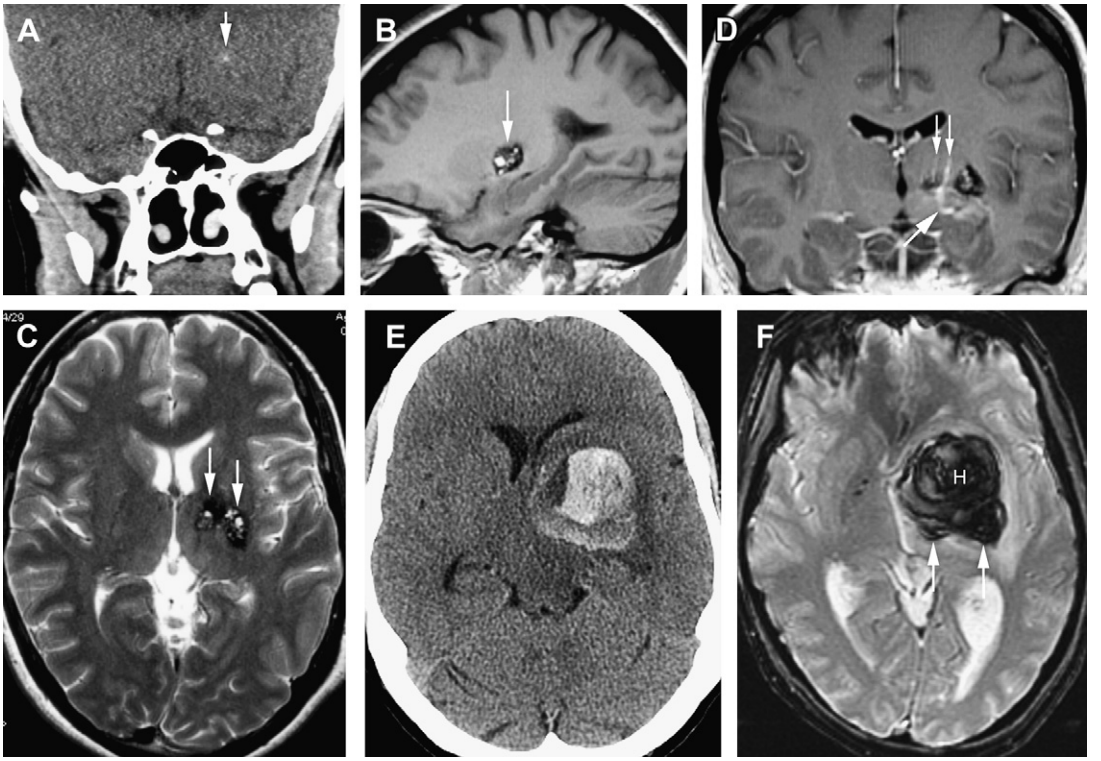

Fig. 11. (*A*) Coronal reconstructed image from an NECT obtained for assessment of sinusitis shows a subtle focus of parenchymal calcification in the region of the deep gray nuclei on the left (*arrow*). (*B*) A sagittal T1W image in the same patient shows a well-circumscribed rounded lesion with heterogeneous high signal in the center and a peripheral rim of hemosiderin staining. This appearance is typical of a CM. (*C*) An axial T2W image in the same patient shows that there are 2 CMs adjacent to each other along the margin of the left thalamus and the left internal capsule. These lesions have the popcorn or mulberrylike appearance of lobulated central T2 hyperintensity and peripheral hypointensity that is typical of CMs. (*D*) Following administration of gadolinium, a coronal T1W image shows a venous malformation adjacent to the CMs, with smaller venous radicles (*thin arrows*) draining into a larger vein (*large thick arrow*). (*E*) Axial NECT 2 years later when the patient developed acute headache and right-sided weakness shows a large acute somewhat heterogeneous hematoma centered in the left putamen and thalamus. (*F*) Axial GRE image shows the acute hematoma (H) with the lobulated CMs (*arrows*) at its posterior aspect. The patient subsequently underwent evacuation of the hematoma and resection of the CMs.

Table 3
Classification schemes for dAVF

Borden Classification	
Type I	Dural arterial supply drains antegrade into venous sinus
Type II	Dural arterial supply drains into venous sinus. High pressure in sinus results in both antegrade drainage and retrograde drainage via cortical veins
Type III	Dural arterial supply drains retrograde into cortical veins
Cognard Classification	
Type I	Drainage into a venous sinus, with normal antegrade flow in sinus
Type II	Drainage into a sinus but with insufficient antegrade venous drainage and reflux. (IIa) retrograde venous drainage into sinus(es) only; (IIb) retrograde venous drainage into cortical vein(s) only; (IIa+b) retrograde venous drainage into sinus (es) and cortical vein(s)
Type III	Direct cortical venous drainage without venous ectasia
Type IV	Direct cortical venous drainage with venous ectasia >5 mm in diameter and 3 times larger than the diameter of the draining vein
Type V	Intracranial fistula drains into spinal perimedullary veins

Data from Borden JA, Wu JK, Shucart WA. A proposed classification for spinal and cranial dural arteriovenous fistulous malformations and implications for treatment. J Neurosurg 1995;82:166–79; and Cognard C, Gobin YP, Pierot L, et al. Cerebral dural arteriovenous fistulas: clinical and angiographic correlation with a revised classification of venous drainage. Radiology 1995;194:671–80.

VENOUS THROMBOSIS

Thrombotic occlusion of the cerebral veins and dural sinuses accounts for approximately 1% to 2% of strokes in adults, but represents a higher proportion of strokes that occur in young patients. Major risk factors for cerebral venous thrombosis include oral contraceptive use and pregnancy, genetic and acquired thrombophilia, malignancy, and infection.[41] The clinical presentation is highly variable and ranges from headache to seizures and focal neurologic deficits to impairment of the level of consciousness. The pathophysiology of injury relates to venous hypertension, which may manifest acutely as localized venous ischemia and infarction, often with complicating parenchymal hemorrhage. Brain parenchymal edema and hemorrhage in particular locations (posterior temporal lobe, parasagittal frontal or parietal lobe, bilateral thalami) should always suggest the diagnosis of venous thrombosis, and imaging studies should be carefully scrutinized for the presence of suggestive or diagnostic findings.

NECT scans are typically performed as the first line of investigation for patients who present emergently. On noncontrast CT, parenchymal edema and hemorrhage may be present if the patient has a venous infarct. Abnormal increased density may be present in thrombosed venous sinuses, as well as in thrombosed cortical veins (the so-called "cord sign").[42] This density decreases after the first week, making the thrombosis more difficult to detect on NECT. Contrast-enhanced CT and CTA are helpful in assessment of possible venous thrombosis, as thrombus appears as a filling defect or segmental lack of opacification in what should be a completely opacified vein or dural sinus.[43] This situation gives rise to the "empty delta" sign, a cardinal sign of dural sinus thrombosis (**Fig. 13**). MR imaging of the brain is more sensitive than CT to the parenchymal edema of venous ischemia and nonhemorrhagic venous infarction, and also shows parenchymal hemorrhage well on T2* sequences (**Fig. 14**). DW images show variable reduced diffusion in venous ischemia/infarction compared with acute arterial infarction, and the lack of reduced diffusion does not exclude venous ischemia/infarction.[44] Routine spin-echo images may show a lack of dural sinus flow void or may show abnormal signal intensity in a thrombosed cortical vein. Some patients may have only a thrombosed cortical vein without associated thrombosis of the dural sinus. This entity has gained more recognition in recent years, and thrombosed cortical veins may be appreciated on NECT or spin-echo or gradient-echo MR images (**Fig. 15**). With venous thrombosis, MRV typically shows a lack of flow-related enhancement in the affected cerebral vein or dural sinus, but one must be careful not to interpret a hypoplastic sinus as a thrombosed sinus. Following gadolinium administration, the MR equivalent of the empty delta sign may be observed in the dural venous sinuses.

The mainstay of treatment of cerebral venous thrombosis is anticoagulation, even in the setting of brain parenchymal hemorrhage. Catheter

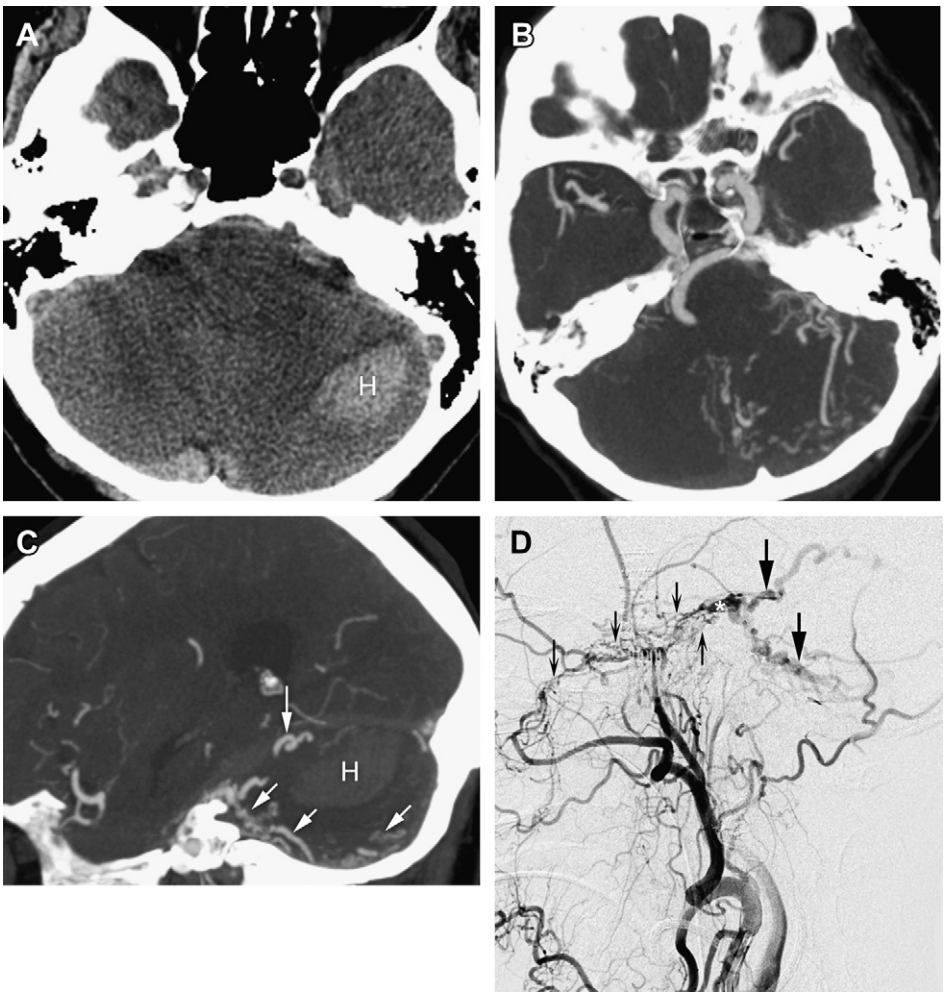

Fig. 12. (*A*) Axial NECT in a middle-aged woman with acute onset of headache and dizziness shows an acute hematoma (H) in the left lateral cerebellum. This is an atypical location for a hypertensive hemorrhage in the cerebellum, because these are usually centered in the deep white matter of the cerebellum. (*B*) Axial MIP from a CTA shows numerous tortuous, corkscrewlike vessels in the posterior fossa, without a discrete nidus. (*C*) Sagittal MIP from the CTA again shows numerous corkscrew vessels in the posterior fossa (*white arrows*), extending along the dural surfaces, as well as the cerebellar hematoma (H). (*D*) A lateral view from a catheter angiogram during injection of the left external carotid artery shows numerous small, irregular arterial feeders (*black arrows*) arising from the middle meningeal artery. The location of the fistulous communication within the dura is indicated by the asterisk (*), and associated enlarged tortuous early draining cortical veins are also seen (*large black arrows*).

angiography generally does not play a role in the diagnosis of cerebral venous thrombosis, but may be indicated for administration of intravenous thrombolytics and for mechanical clot lysis as a rescue therapy in patients with a fulminant course or in those who continue to worsen in spite of systemic anticoagulation.

NEOPLASIA

Primary and metastatic brain tumors may have associated ICH, occurring in up to 15% of patients, but rarely is hemorrhage the presenting symptom of a previously undiagnosed brain mass.[45] In this circumstance, the diagnosis of an underlying tumor may pose diagnostic difficulties, especially if the tumor is small compared with the volume of the brain hematoma. Although many malignant gliomas show microscopic evidence of hemorrhage, acute hemorrhage as the presenting sign of a malignant glioma is most common with glioblastoma multiforme. The intracerebral metastases that are most likely to hemorrhage are those caused by choriocarcinoma, melanoma, thyroid carcinoma, and renal cell carcinoma, although most hemorrhagic

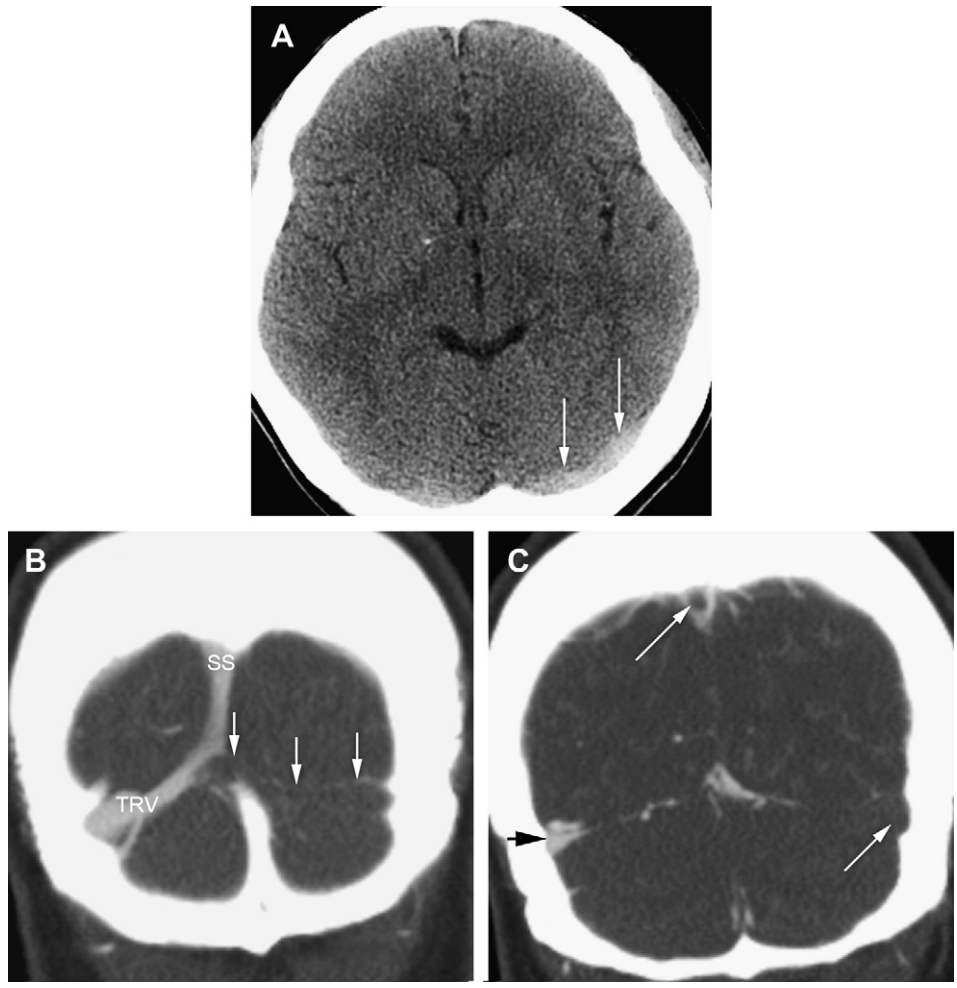

Fig. 13. (*A*) Axial NECT in a young woman with headache shows increased density along the course of the left transverse sinus. (*B*) A coronal reconstructed image from a CTA shows normal opacification of the superior sagittal sinus and right transverse sinus on this slice; the thrombosed left transverse sinus (*white arrows*) does not opacify with contrast, and thrombus extends medially to the torcular herophili. (*C*) A more anterior coronal image shows not only the thrombosis at the level of the left transverse-sigmoid junction (*lower white arrow*), but also a filling defect in the superior sagittal sinus, consistent with partial thrombosis at this level (*upper white arrow*) and demonstrating the "empty delta" sign. The normal right transverse-sigmoid junction is indicated (*black arrow*).

metastases are caused by breast and lung carcinomas because these are more common causes of brain metastases in the general population. Another entity to consider is atrial myxoma, which may give rise to oncotic intracranial aneurysms with secondary subarachnoid and/or parenchymal hemorrhage.

Certain imaging findings have been described as more consistent with malignant or intratumoral cerebral hemorrhage.[46] Most of these findings are applicable to MR, as CT scans most commonly show areas of nonspecific hemorrhage (**Fig. 16**). However, more perihematoma edema on the CT scan than one would expect from the ICH alone should raise suspicion for an underlying malignancy, as should marked heterogeneity of the hematoma. On MR imaging, intratumoral hemorrhages tend to be extremely heterogeneous because of blood products in varying phases of signal evolution, debris-fluid levels, and/or the presence of edema, tumor, and necrotic tissue mixing with blood products. These lesions often show associated regions of nonenhancing or enhancing nonhemorrhagic tumor tissue (**Fig. 17**), and any surrounding hypointense rim of ferritin or hemosiderin may be incomplete or irregular. If the hematoma is followed over time because of uncertainty about its benign or malignant nature, then it

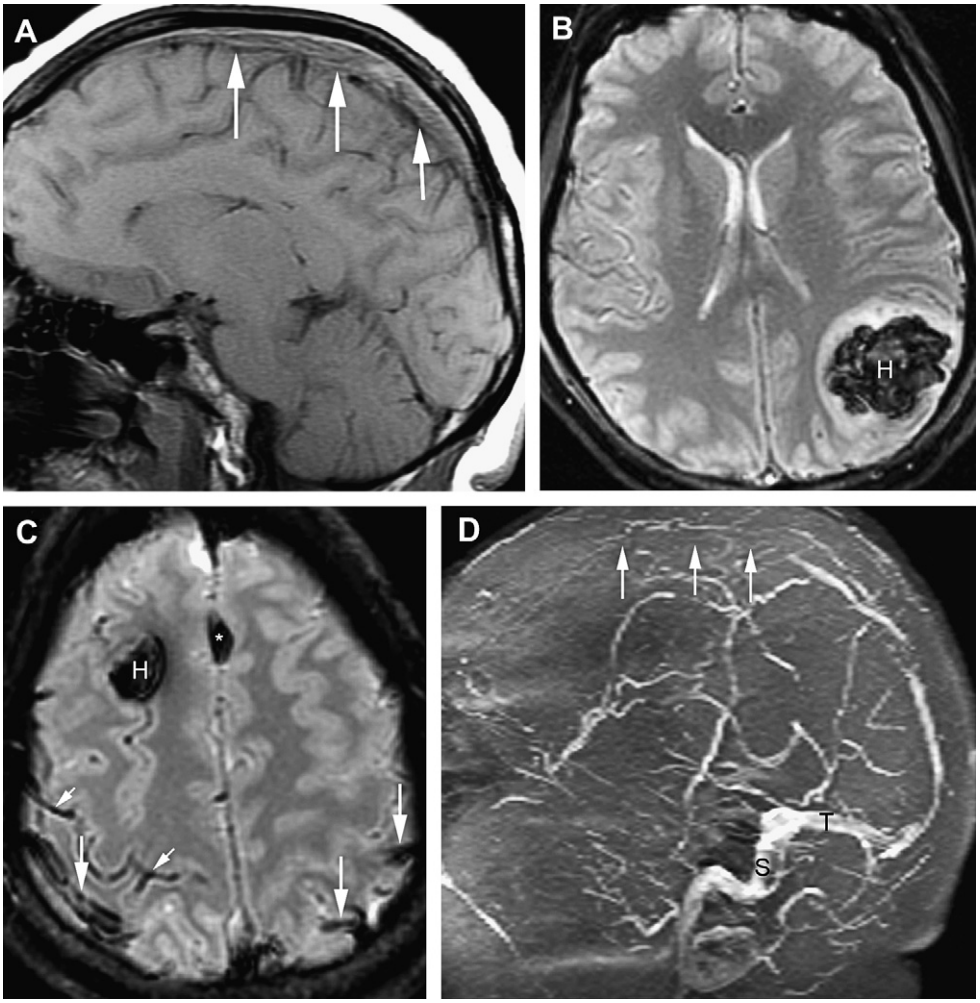

Fig. 14. (*A*) Sagittal T1W image shows abnormal increased signal intensity in the superior sagittal sinus (*white arrows*), consistent with thrombosis. Normally, a flow void would be expected in the sagittal sinus on a spin-echo image. (*B*) Axial GRE image shows a left parietal intraparenchymal hemorrhage (H) with associated edema, consistent with hemorrhagic venous infarction. (*C*) A more superior GRE image shows an additional hematoma (H) in the right frontal lobe, as well as areas of SAH (*small white arrows*). Several thrombosed cortical veins heading toward the sagittal sinus are also appreciated (*large white arrows*). (*D*) A lateral projection from an MR venogram shows a lack of flow-related enhancement in the superior sagittal sinus (*white arrows*). Flow-related enhancement is seen in the transverse (T) and sigmoid (S) sinuses.

may show delayed evolution of blood breakdown products and persistent edema and mass effect, even in late stages of evolution. The identification of additional enhancing lesions in the brain may be helpful in making the diagnosis of metastatic disease, and in some cases a systemic staging workup with body CT and/or fluorodeoxyglucose positron emission tomography CT may be indicated to assess for a primary lesion as well as other metastatic sites of disease.

VASCULITIS/VASCULOPATHY/VASOSPASM

Primary vascular abnormalities such as vasculitis, nonatherosclerotic vasculopathy, and vasoconstrictive syndromes may on occasion present with spontaneous hemorrhages that may be parenchymal or subarachnoid in location.[47] Central nervous system (CNS) vasculitis may be primary or secondary to systemic vasculitides and often presents with headache, confusion,

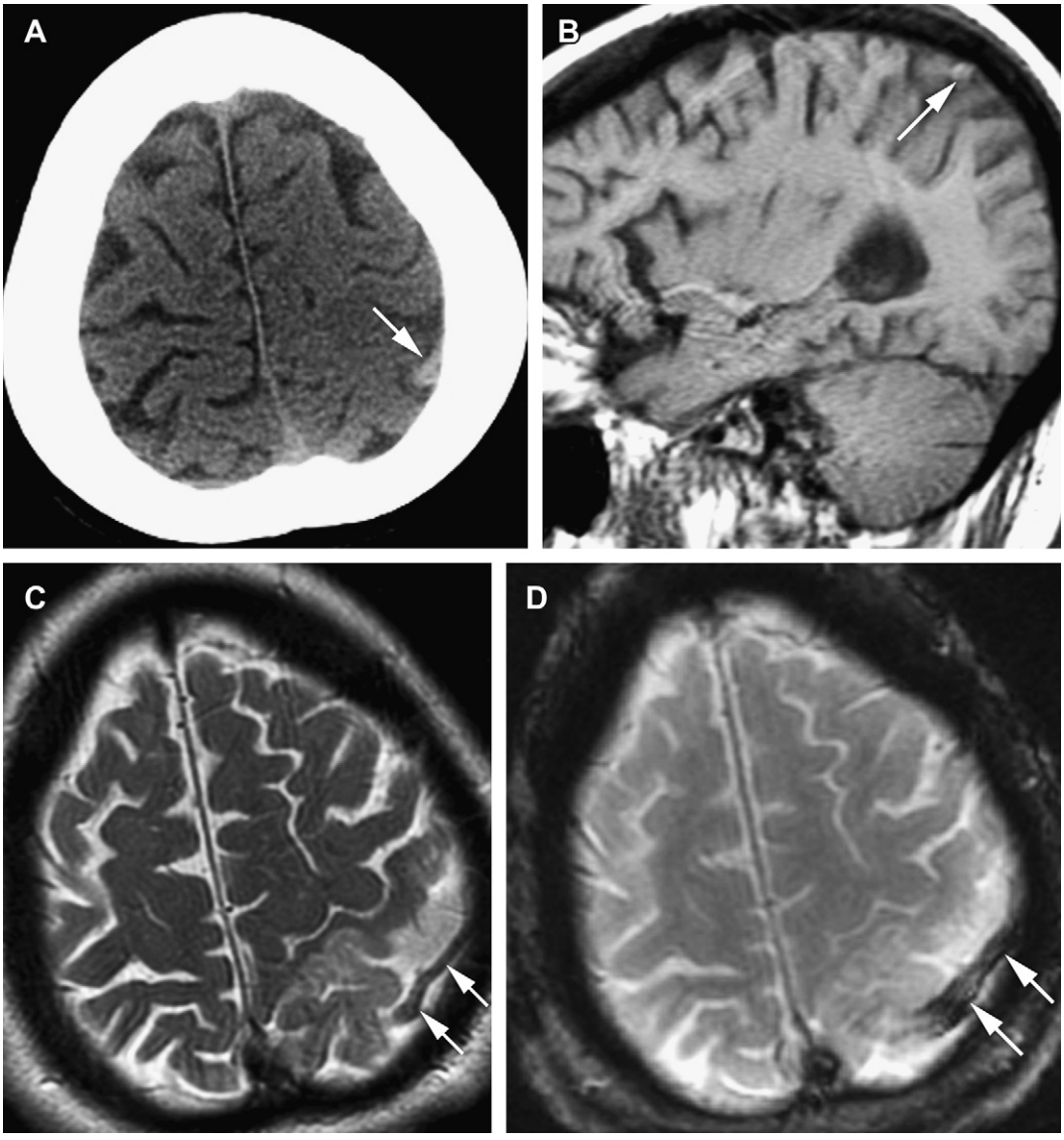

Fig. 15. (*A*) Axial NECT in a young woman with headache and right arm sensory deficits shows a tubular structure of increased density, consistent with a thrombosed cortical vein. The underlying brain parenchyma shows hypodensity and crowding of sulci, consistent with parenchymal edema caused by localized venous hypertension. (*B*) A sagittal T1W image shows high signal intensity in a thrombosed cortical vein overlying the left parietal lobe. (*C*) An axial fast spin-echo T2W image shows to better advantage the left parietal vasogenic edema, as well as the thrombosed cortical vein (*white arrows*). (*D*) An axial GRE image shows blooming of the clot within the left parietal cortical vein caused by magnetic susceptibility effects of the acute clot.

seizure, and focal neurologic deficits. MR imaging typically shows multifocal areas of T2 signal abnormality involving the deep gray nuclei and subcortical white matter, accompanied by reduced diffusion in the acute stage of injury and variable enhancement after gadolinium. CTA and MRA may show vascular irregularity, particularly if larger vessels are involved, but these modalities are relatively insensitive to small vessel involvement, and catheter angiography is often indicated for further evaluation. The hallmark of vasculitis on cerebral angiography is multifocal areas of vascular stenosis and dilatation involving small and medium-sized vessels; sometimes this can be difficult to differentiate from intracranial atherosclerosis, and the overall presentation of the

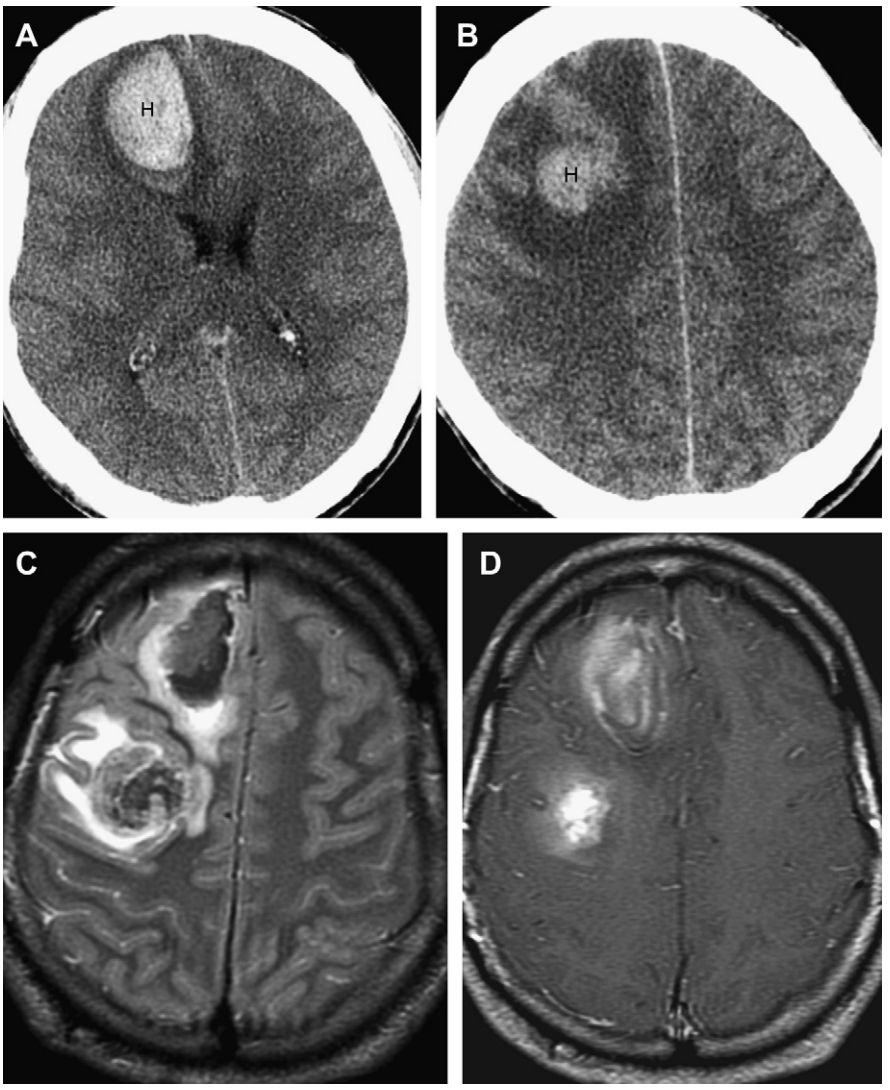

Fig. 16. (*A*) Axial NECT in a young man with acute onset of headache shows a right frontal lobar hematoma (H) with mild surrounding vasogenic edema. (*B*) A more superior NECT shows a second hematoma (H) associated with a larger amount of vasogenic edema. This amount of edema would not be expected for a hyperacute benign hematoma. (*C*) Axial T2W image from an MR scan acquired shortly after the CT shows 2 right frontal hematomas with heterogeneous signal intensity and associated vasogenic edema. (*D*) Axial T1W postgadolinium image shows heterogeneous high signal intensity associated with the hematomas, most of which was present before gadolinium administration. In this patient the suspicion for underlying neoplasia was high, and metastatic choriocarcinoma was confirmed when the lesions were surgically decompressed.

patient must be considered in assigning a diagnosis of CNS vasculitis in the absence of biopsy confirmation of this diagnosis.

Most nonatherosclerotic vasculopathies present with ischemic lesions, but intracerebral hemorrhage may be a presenting or complicating feature of these disorders. Moyamoya disease and moyamoya syndrome are characterized by progressive stenosis of the intracranial internal carotid arteries (ICAs) and their proximal branches. Most patients in the United States present with ischemic symptoms, although hemorrhage may be the presenting sign in as many as 20% of adults.[48] These hemorrhages may be intraparenchymal (often basal ganglia), intraventricular, or subarachnoid in location (**Fig. 18**). Bleeding is usually attributed to rupture of fragile collateral vessels, although shifting circulation patterns may lead to formation of cerebral

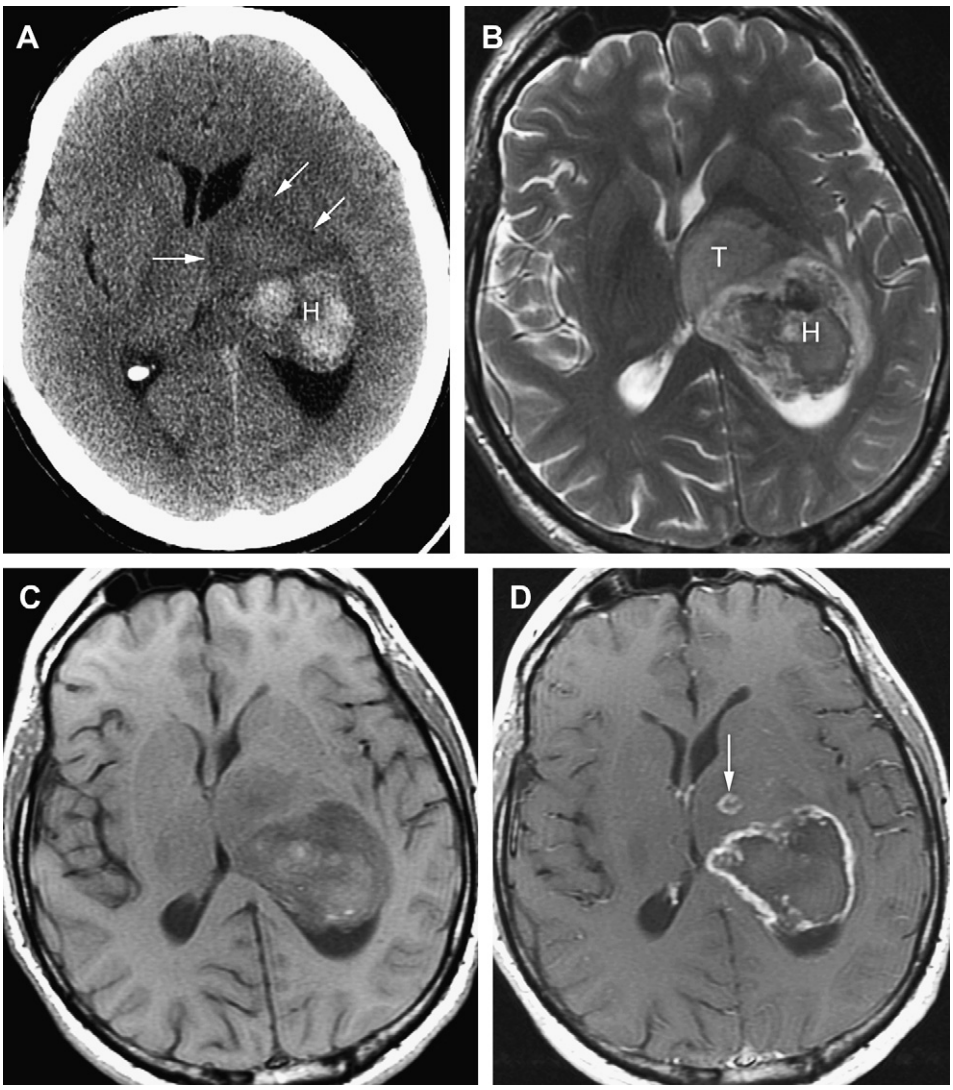

Fig. 17. (*A*) Axial NECT in a young man with headache and right-sided motor and sensory deficits shows a hematoma (H) in the posterior left thalamus. The hematoma is somewhat heterogeneous and is associated with a large area of hypodensity anteriorly (*white arrows*). Edema and mass effect are present, as well as trapping of the left ventricular atrium. (*B*) An axial T2W image shows that the hematoma (H) has heterogeneous signal intensity. More anteriorly, abnormal T2 hyperintensity is present in the thalamus, suggestive of nonenhancing infiltrative tumor (T). (*C*) An axial T1W image again shows the atypical hematoma as well as the more anterior infiltrative tissue. (*D*) Following administration of gadolinium, an axial T1W image shows irregular peripheral enhancement around the hemorrhagic component of the tumor, as well as focal nodular enhancement (*arrow*) more anteriorly within the thalamus. Subsequent hematoma evacuation and biopsy confirmed glioblastoma multiforme.

aneurysms (often of the posterior circulation) and this may be another cause of hemorrhage in patients with moyamoya. MRI/MRA studies in moyamoya typically show ischemic lesions, often in a watershed distribution, as well as unilateral or bilateral supraclinoid ICA stenosis or occlusion and dilated lenticulostriate collateral vessels; MR perfusion studies are typically abnormal, with decreased flow in the affected vascular territories. Management of moyamoya often requires direct or indirect revascularization procedures.[49]

Reversible cerebral vasoconstriction syndrome (RCVS) is increasingly recognized as a cause of ischemic and hemorrhagic lesions of the brain.[50] It is characterized by prolonged but reversible vasoconstriction of the cerebral arteries and typically presents with thunderclap headache, with or without focal neurologic symptoms or signs.

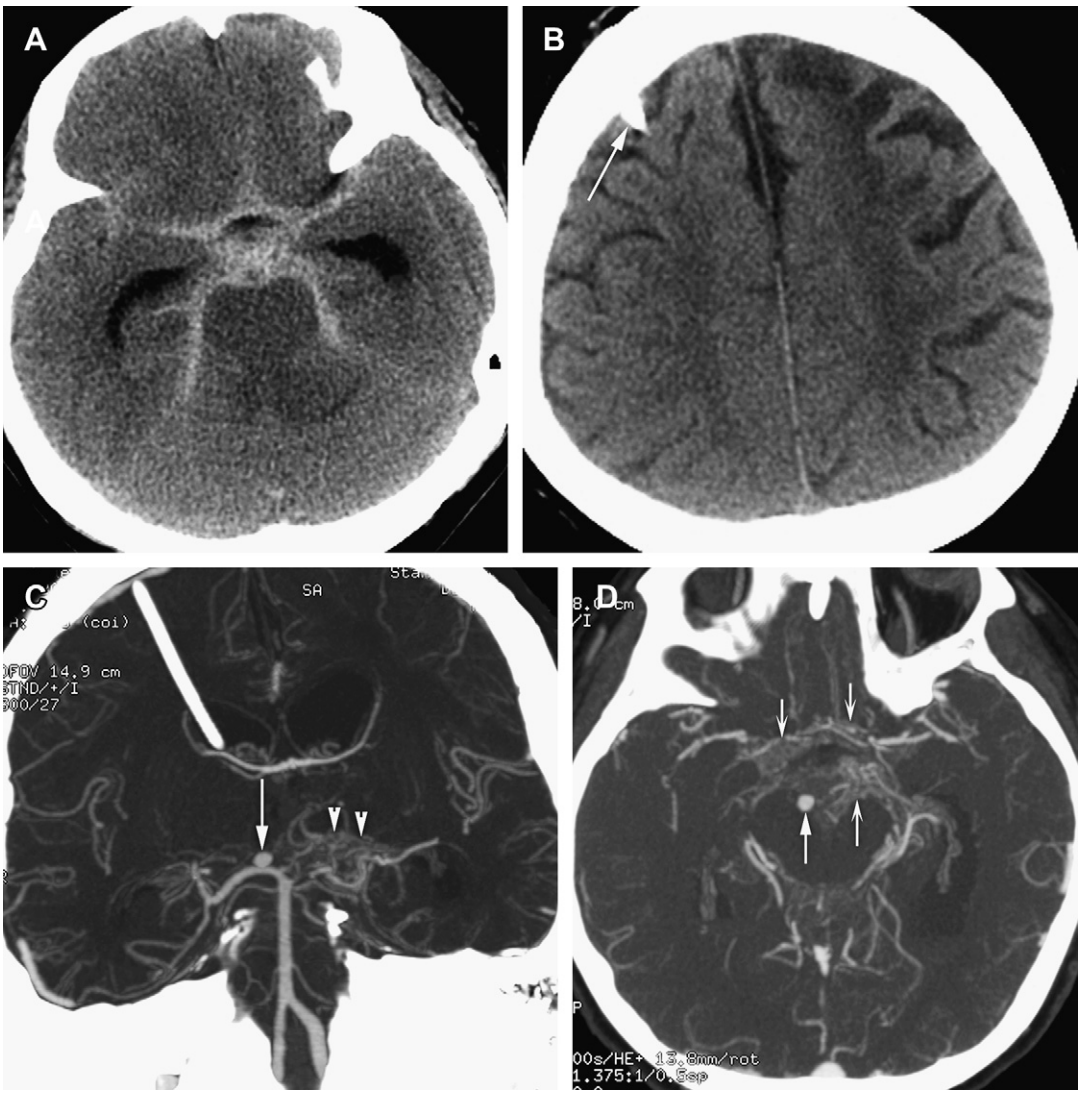

Fig. 18. (*A*) Axial NECT shows extensive SAH in the basal cisterns of a 48-year-old woman, as well as ventricular enlargement consistent with hydrocephalus. (*B*) A more superior NECT shows part of a right external ventricular drain (*arrow*), as well as left frontal encephalomalacia suggesting a remote ischemic insult, although the patient and her family reported no history of stroke. (*C*) Coronal MIP image from a CTA shows a saccular aneurysm (*large white arrow*) arising from the right P1 segment of the posterior cerebral artery, which is an unusual location for a saccular aneurysm. The image also shows poor visualization of the left P1 segment and instead shows a tangle of small collateral vascular channels (*arrowheads*). An external ventricular drain is present with its tip in the right frontal horn. (*D*) An axial MIP image from the CTA again shows the saccular right P1 aneurysm (*straight white arrow*). Numerous small collateral vessels are seen throughout the suprasellar cistern (*concave white arrows*); in addition, the proximal M1 segments of the MCAs are poorly seen bilaterally, and the A1 segments of the ACAs are diminutive. These findings are consistent with advanced moyamoya disease.

This entity has previously been known by a variety of names, including Call-Fleming syndrome and benign or reversible angiitis of the CNS. Associated conditions include eclampsia, use of amphetamines and other sympathomimetics, use of serotonergic drugs, and a history of migraine or other headache syndromes.[51] CT and MR images of these patients may show areas of ischemic infarction and/or hemorrhage (**Fig. 19**); CTA and MRA examinations may show diffuse vascular irregularity, although this may be difficult to differentiate from motion or a poor bolus (ie, artifactual causes of apparent vascular irregularity) on these noninvasive studies. Catheter angiography shows

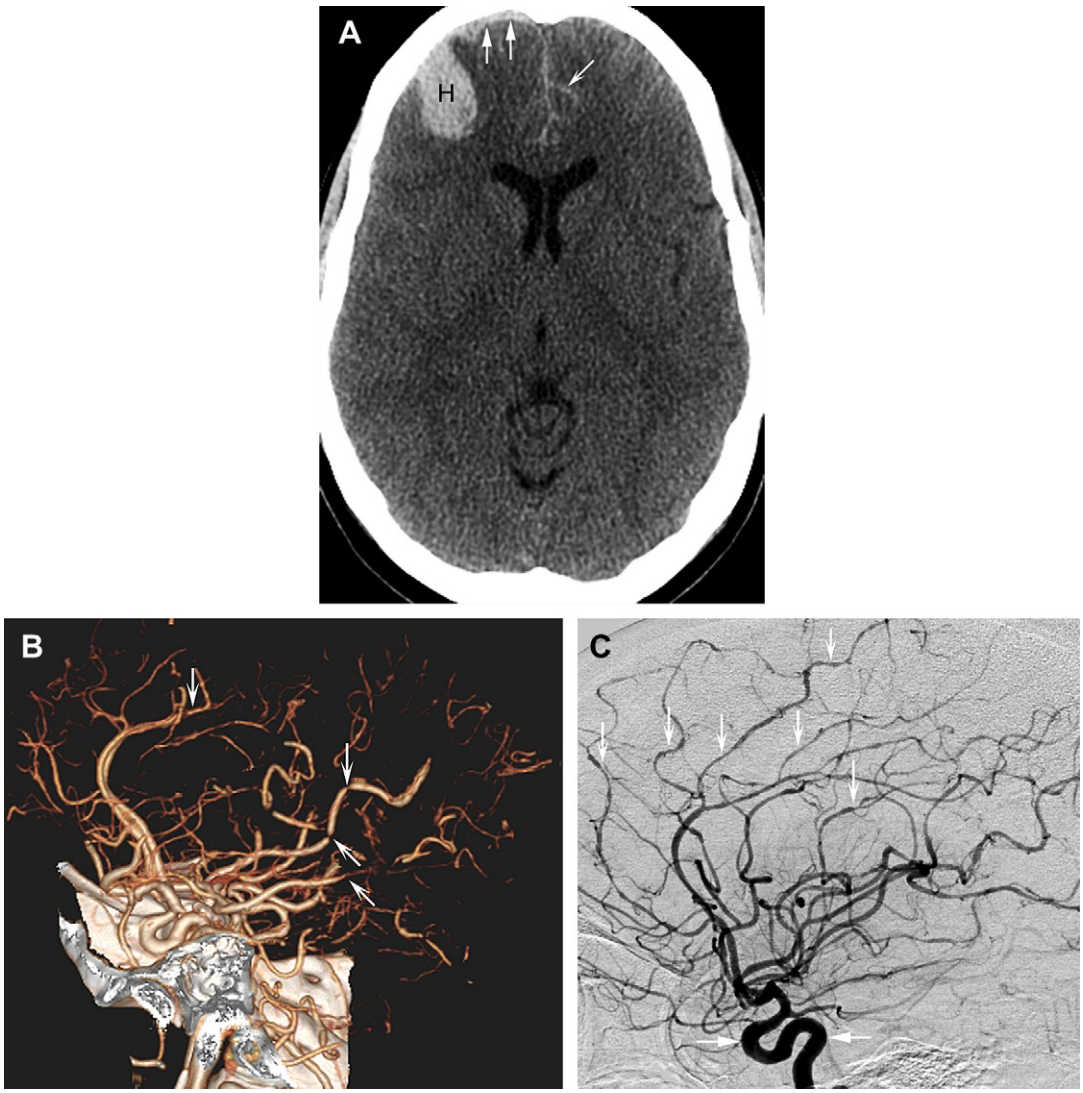

Fig. 19. (*A*) Axial NECT image from a middle-aged woman with acute onset of severe headache shows a right frontal lobar hematoma (H), as well as a small subdural hematoma (*straight white arrows*) and subarachnoid blood (*concave arrow*) interdigitating into frontal sulci. (*B*) A 3D reconstruction of the intracranial vasculature from a CTA shows numerous sites of vascular irregularity and narrowing (*arrows*), but it is difficult to be sure if the vessels are truly abnormal or if a poor bolus could be influencing the appearance of the peripheral arterial branches. (*C*) A lateral view from a catheter angiogram with injection of the left ICA shows normal proximal vessels, with a normal carotid siphon (*large white arrows*). Peripherally, however, MCA and ACA branches show extensive multifocal sites of vascular irregularity and narrowing (*concave white arrows*). In the past this would likely have been interpreted as CNS vasculitis, but this patient improved markedly with only supportive care and calcium channel blockers. These clinical and radiographic findings were interpreted as consistent with RCVS.

diffuse irregularity of the cerebral vasculature that mimics CNS vasculitis. However, these patients have a more benign course and often improve spontaneously in several weeks; some have improved more rapidly with calcium channel blockers. It is essential to consider RCVS in the differential diagnosis before a patient is put on aggressive therapy such as steroids and cyclophosphamide for presumed CNS vasculitis. Vascular changes have also been described in posterior reversible encephalopathy syndrome (PRES), and the relationship between PRES and RCVS, if any, remains to be elucidated.[52]

SUBDURAL HEMORRHAGE

Spontaneous hemorrhage into the subdural space may be seen with intracranial hypotension[53,54] and

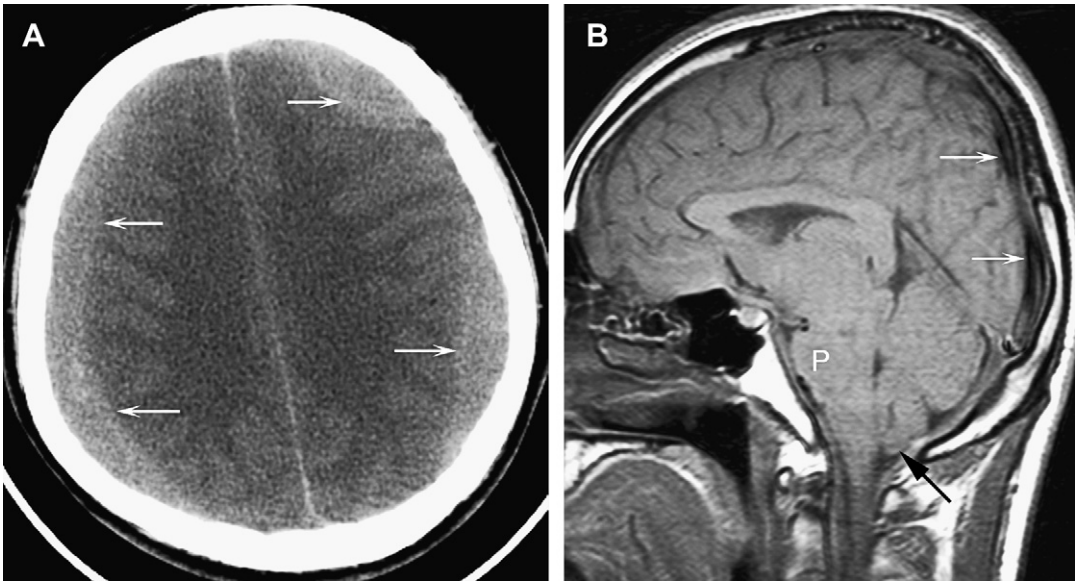

Fig. 20. (*A*) An axial NECT scan in a young woman with postural headache for several weeks and now altered mental status shows bilateral subacute holohemispheric subdural hematomas. (*B*) A midline sagittal T1W image from an MR scan in the same patient shows downward displacement of the diencephalon and mesencephalon, flattening of the pons (P) against the clivus, and crowding of the foramen magnum (*black arrow*). The superior sagittal sinus is patent and prominent, consistent with intracranial hypotension; if intracranial hypertension were present, then one would expect the venous sinus to be small. This patient underwent evacuation of her subdural hematomas and her intracranial hypotension resolved after 2 epidural blood patches.

also with hemorrhagic dural metastases; clotting disorders may also lead to spontaneous subdural hematoma (SDH). Spontaneous intracranial hypotension is further discussed in the article Intracranial Hypo- and Hypertension by Yuh and Dillon elsewhere in this issue, but in brief, the downward displacement of the brain that occurs in spontaneous intracranial hypotension may lead to stretching and eventually tearing of the bridging cortical veins, resulting in frank subdural hemorrhage (**Fig. 20**) rather than just vascular engorgement of the dura. SDH is a rare presentation of intracranial metastatic disease, but has been described in the setting of several cancers, notably breast carcinoma and choriocarcinoma.[55]

OTHER CONDITIONS ASSOCIATED WITH ICH

Many other conditions may be associated with spontaneous ICH, including the use of anticoagulants (even in the absence of trauma or hypertension), clotting factor deficiencies, hepatic dysfunction, metabolic disorders, and viral encephalitides. Excellent communication between the radiologist and the referring physician can help to determine the cause of a spontaneous ICH, although in some patients the cause remains uncertain despite an extensive clinical and diagnostic imaging workup in the acute and chronic phase.

REFERENCES

1. Barkovich AJ, Atlas SW. Magnetic resonance imaging of intracranial hemorrhage. Radiol Clin North Am 1988;26:801–20.
2. Atlas SW, Thulborn KR. MR detection of hyperacute parenchymal hemorrhage of the brain. AJNR Am J Neuroradiol 1998;19:1471–507.
3. Parizel PM, Makkat S, Van Miert E, et al. Intracranial hemorrhage: principles of CT and MRI interpretation. Eur Radiol 2001;11:1770–83.
4. Sessa M. Intracerebral hemorrhage and hypertension. Neurol Sci 2008;29:S258–9.
5. Kinoshita T, Okudera T, Tamura H, et al. Assessment of lacunar hemorrhage associated with hypertensive stroke by echo-planar gradient-echo T2*-weighted MRI. Stroke 2000;31:1646–50.
6. Brott T, Broderick J, Kothari R, et al. Early hemorrhage growth in patients with intracerebral hemorrhage. Stroke 1997;28:1–5.
7. Cucchiara B, Messe S, Sansing L, et al. CHANT Investigators. Hematoma growth in oral anticoagulant related intracerebral hemorrhage. Stroke 2008; 39:2993–6.

8. Fujii Y, Takeuchi S, Sasaki O, et al. Multivariate analysis of predictors of hematoma enlargement in spontaneous intracerebral hemorrhage. Stroke 1998;29:1160–6.
9. Wada R, Aviv RI, Fox AJ, et al. CT angiography "spot sign" predicts hematoma expansion in acute intracerebral hemorrhage. Stroke 2007;38:1257–62.
10. Goldstein JN, Fazen LE, Snider R, et al. Contrast extravasation on CT angiography predicts hematoma expansion in intracerebral hemorrhage. Neurology 2007;68:889–94.
11. Kim J, Smith A, Hemphill JC III, et al. Contrast extravasation on CT predicts mortality in primary intracerebral hemorrhage. AJNR Am J Neuroradiol 2008;29:520–5.
12. Broderick J, Connolly S, Feldmann E, et al. Guidelines for the management of spontaneous intracerebral hemorrhage in adults: 2007 update: a guideline from the American Heart Association/American Stroke Association Stroke Council, High Blood Pressure Research Council, and the Quality of Care and Outcomes in Research Interdisciplinary Working Group. Circulation 2007;116(16):e391–413.
13. Mendelow AD, Gregson BA, Fernandes HM, et al. Early surgery versus initial conservative treatment in patients with spontaneous supratentorial intracerebral haematomas in the International Surgical Trial in Intracerebral Haemorrhage (STICH): a randomised trial. Lancet 2005;365:387–97.
14. Zhang-Nunes SX, Maat-Schieman ML, van Duinen SG, et al. The cerebral beta-amyloid angiopathies: hereditary and sporadic. Brain Pathol 2006;16:30–9.
15. Pezzini A, Padovani A. Cerebral amyloid angiopathy-related hemorrhages. Neurol Sci 2008;29:S260–3.
16. Knudsen KA, Rosand J, Karluk D, et al. Clinical diagnosis of cerebral amyloid angiopathy: validation of the Boston criteria. Neurology 2001;56:537–9.
17. Tsui YK, Tsai FY, Hasso AN, et al. Susceptibility-weighted imaging for the differential diagnosis of cerebral vascular pathology: a pictorial review. J Neurol Sci 2009;287(1–2):7–16.
18. Rosand J, Hylek EM, O'Donnell HC, et al. Warfarin-associated hemorrhage and cerebral amyloid angiopathy: a genetic and pathologic study. Neurology 2000;55:947–51.
19. Tsivgoulis G, Frey JL, Flaster M, et al. Pre-tissue plasminogen activator blood pressure levels and risk of symptomatic intracerebral hemorrhage. Stroke 2009;40:3631–4.
20. Aviv RI, D'Esterre CD, Murphy BD, et al. Hemorrhagic transformation of ischemic stroke: prediction with CT perfusion. Radiology 2009;250:867–77.
21. Lansberg MG, Thijs VN, Bammer R, et al. Risk factors of symptomatic intracerebral hemorrhage after tPA therapy for acute stroke. Stroke 2007;38:2275–8.
22. Albers GW, Thijs VN, Wechsler L, et al. Magnetic resonance imaging profiles predict clinical response to early reperfusion: the diffusion and perfusion imaging evaluation for understanding stroke evolution (DEFUSE) study. Ann Neurol 2006;60:508–17.
23. Khatri P, Wechsler LR, Broderick JP. Intracranial hemorrhage associated with revascularization therapies. Stroke 2007;38(2):431–40.
24. Lansberg MG, Albers GW, Wijman CA. Symptomatic intracerebral hemorrhage following thrombolytic therapy for acute ischemic stroke: a review of the risk factors. Cerebrovasc Dis 2007;24:1–10.
25. Singer OC, Humpich MC, Fiehler J, et al. Risk for symptomatic intracerebral hemorrhage after thrombolysis assessed by diffusion-weighted magnetic resonance imaging. Ann Neurol 2008;63:52–60.
26. Ruttmann E, Willeit J, Ulmer H, et al. Neurological outcome of septic cardioembolic stroke after infective endocarditis. Stroke 2006;37:2094–9.
27. Chen W, Wang J, Xin W, et al. Accuracy of 16-row multislice computed tomographic angiography for assessment of small cerebral aneurysms. Neurosurgery 2008;62:113–22.
28. McKinney AM, Palmer CS, Truwit CL, et al. Detection of aneurysms by 64-section multidetector CT angiography in patients acutely suspected of having an intracranial aneurysm and comparison with digital subtraction and 3D rotational angiography. AJNR Am J Neuroradiol 2008;29:594–602.
29. Yoon DY, Lim KJ, Choi CS, et al. Detection and characterization of intracranial aneurysms with 16-channel multidetector row CT angiography: a prospective comparison of volume-rendered images and digital subtraction angiography. AJNR Am J Neuroradiol 2007;28:60–7.
30. Hochmuth A, Spetzger U, Schumacher M. Comparison of three-dimensional rotational angiography with digital subtraction angiography in the assessment of ruptured cerebral aneurysms. AJNR Am J Neuroradiol 2002;23:1199–205.
31. White PM, Teasdale EM, Wardlaw JM, et al. Intracranial aneurysms: CT angiography and MR angiography for detection. Prospective blinded comparison in a large patient cohort. Radiology 2001;219:739–49.
32. Chaudhary SR, Ko N, Dillon WP, et al. Prospective evaluation of multidetector row CT angiography for the diagnosis of vasospasm following subarachnoid hemorrhage: a comparison with digital subtraction angiography. Cerebrovasc Dis 2008;25:144–50.
33. Al-Shahi R, Warlow C. A systematic review of the frequency and prognosis of arteriovenous malformations of the brain in adults. Brain 2001;124:1900–26.
34. Spetzler RF, Martin NA. A proposed grading system for arteriovenous malformation. J Neurosurg 1986;65:476–83.
35. Al-Shahi Salman R, Berg MJ, Morrison L, et al. Hemorrhage from cavernous malformations of the brain. Stroke 2008;39:3222–30.

36. Wilson M, Enevoldson P, Menezes B. Intracranial dural arterio-venous fistula. Pract Neurol 2008;8:362–9.
37. Zipfel GJ, Shah MN, Refai D, et al. Cranial dural arteriovenous fistulas: modification of angiographic classification scales based on new natural history data. Neurosurg Focus 2009;26:E14.
38. Borden JA, Wu JK, Shucart WA. A proposed classification for spinal and cranial dural arteriovenous fistulous malformations and implications for treatment. J Neurosurg 1995;82:166–79.
39. Cognard C, Gobin YP, Pierot L, et al. Cerebral dural arteriovenous fistulas: clinical and angiographic correlation with a revised classification of venous drainage. Radiology 1995;194:671–80.
40. Farb RI, Agid R, Willinsky RA, et al. Cranial dural arteriovenous fistula: diagnosis and classification with time-resolved MR angiography at 3T. AJNR Am J Neuroradiol 2009;30:1546–51.
41. English JD, Fields JD, Le S, et al. Clinical presentation and long-term outcome of cerebral venous thrombosis. Neurocrit Care 2009;11(3):330–7.
42. Linn J, Pfefferkorn T, Ivanicova K, et al. Noncontrast CT in deep cerebral venous thrombosis and sinus thrombosis: comparison of its diagnostic value for both entities. AJNR Am J Neuroradiol 2009;30: 728–35.
43. Linn J, Ertl-Wagner B, Seelos KC, et al. Diagnostic value of multidetector-row CT angiography in the evaluation of thrombosis of the cerebral venous sinuses. AJNR Am J Neuroradiol 2007;28:946–52.
44. Makkat S, Stadnik T, Peeters E, et al. Pathogenesis of venous stroke: evaluation with diffusion- and perfusion-weighted MRI. J Stroke Cerebrovasc Dis 2003;12:132–6.
45. Salmaggi A, Erbetta A, Silvani A, et al. Intracerebral haemorrhage in primary and metastatic brain tumours. Neurol Sci 2008;29:S264–5.
46. Atlas SW, Grossman RI, Gomori JM, et al. Hemorrhagic intracranial malignant neoplasms: spin-echo MR imaging. Radiology 1987;164:71–7.
47. Refai D, Botros JA, Strom RG, et al. Spontaneous isolated convexity subarachnoid hemorrhage: presentation, radiological findings, differential diagnosis, and clinical course. J Neurosurg 2008;109:1034–41.
48. Scott RM, Smith ER. Moyamoya disease and moyamoya syndrome. N Engl J Med 2009;360:1226–37.
49. Guzman R, Lee M, Achrol A, et al. Clinical outcome after 450 revascularization procedures for moyamoya disease. J Neurosurg 2009;111(5):927–35.
50. Santos E, Zhang Y, Wilkins A, et al. Reversible cerebral vasoconstriction syndrome presenting with haemorrhage. J Neurol Sci 2009;276:189–92.
51. Ducros A, Boukobza M, Porcher R, et al. The clinical and radiological spectrum of reversible cerebral vasoconstriction syndrome. A prospective series of 67 patients. Brain 2007;130:3091–101.
52. Bartynski WS, Boardman JF. Catheter angiography, MR angiography, and MR perfusion in posterior reversible encephalopathy syndrome. AJNR Am J Neuroradiol 2008;29:447–55.
53. Gordon N. Spontaneous intracranial hypotension. Dev Med Child Neurol 2009;51:932–5.
54. Schievink WI. Spontaneous spinal cerebrospinal fluid leaks. Cephalalgia 2008;28:1345–56.
55. Rocque BG, Baskaya MK. Spontaneous acute subdural hematoma as an initial presentation of choriocarcinoma: a case report. J Med Case Reports 2008;2:211.